Strategies for Optimizing Information Extraction from Cortical Recordings

by

Nicholas Brandon Langhals

**A dissertation submitted in partial fulfillment
of the requirements for the degree of
Doctor of Philosophy
(Biomedical Engineering)
in the University of Michigan
2011**

Doctoral Committee:

**Professor Daryl R. Kipke, Chair
Professor Euisik Yoon
Assistant Professor Parag G. Patil
Assistant Professor William Charles Stacey**

Table of Contents

List of Figures

List of Tables

Chapter I

Introduction

I. Overview

Penetrating neural probe technologies provide researchers with the capability to stimulate and record chemical and electrical signals in the brain. While present technology has yielded significant insight into the function of the brain, this technology is limited in a number of ways. Although recent breakthroughs have enabled the fabrication of three dimensional probes with hundreds of recording sites, information processing strategies to utilize this new technology are currently unrealized. Moreover, increasing channel numbers creates larger devices and concurrently highlights data processing and classification problems. Analyzing more channels not only takes more time, but also precludes many of the user-directed sorting and analysis schemes that are commonly used.

Optimizing the information extracted from neural recording electrodes is a key step in increasing the utility, reliability, and longevity of brain machine interfaces

(BMIs) (Gage, Ludwig et al. 2005; Hochberg, Serruya et al. 2006; Lebedev and Nicolelis 2006). A standard BMI can be divided into four separate stages (Figure I-1). First, the neural activity from various sources in the brain is translated into a recorded electrical signal. Next, the recordings are sent through a feature extraction algorithm to reduce the neural recordings into input parameters considered relevant to a BMI. High-speed recordings are typically reduced to individual or multi-unit neuronal firing rates, whereas local field potentials, electrocorticogram (ECoG), and electroencephalogram (EEG) recordings are primarily translated into root mean square (RMS) voltage or segmented into power across specific frequency bands. Third, the extracted neuronal features of interest are decoded into a neural output control signal, typically by obtaining an *a priori* map of the linear relationship between the extracted neural features and a movement parameter. Finally, the neural output control signal is transformed into an electrical signal suitable for driving a neural prosthetic device. Improvements to BMI systems are generally made by making modifications at one of these four stages. The four specific aims outlined for this dissertation are focused on the first two stages: (1) improving the quantity of neural signals being extracted from the brain and (2) advancing the feature extraction techniques for optimizing the usage of the spike data that has been recorded.

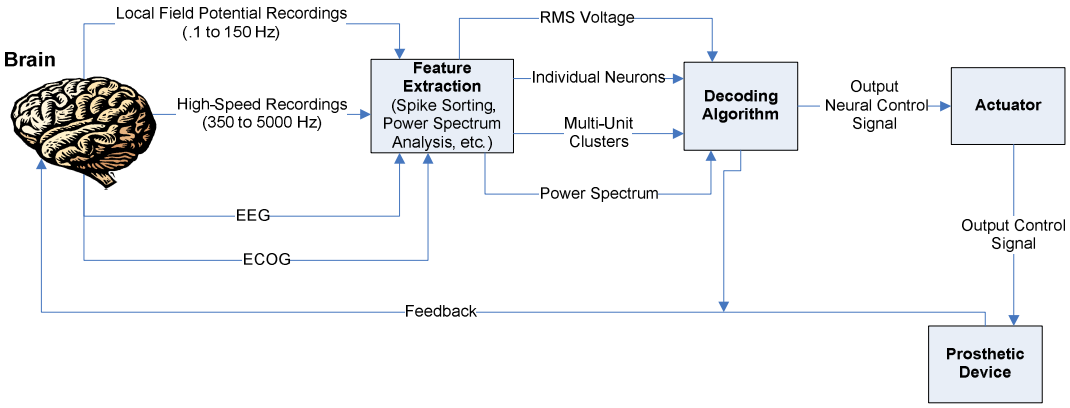

Figure I-1: Taxonomy of a Standard Brain-Machine Interface (BMI)

II. Historical Development of Probe Technologies

One of the earliest experiments involving extracellular electrophysiological recording of the neural environment was performed in the 1950's (Strumwasser 1958). Prior experiments had required the use of intracellular electrode types and penetrations that, while useful in tissue slices or on the surface of the brain, are too complicated to use for chronic evaluation of changes in the behavior of neurons. Following this work, individual microwires were assembled into arrays so that multiple locations within a region of the brain could be sampled simultaneously. The electrodes used in these studies were insulated hard metal wires with the tip exposed to create a metal interface to the brain (Olds, Disterhoft et al. 1972), or etched to a sharpened tip (Marg and Adams 1967; Burns, Stean et al. 1974). Both of these processes yield inherent variability in electrode shape, size, and functionality. Chronic evaluation of these devices also yields variable performance that can degrade to unusable levels within weeks of implantation (Williams, Rennaker et al. 1999).

The first generation of microfabricated neural probes were developed by Kensall Wise in the 1970's (Williams, Rennaker et al. 1999). As compared to the variable designs and yields present in the cutting and etching of microwires, these devices were based on the processes similar to those used in integrated circuits. The reproducibility and consistency of the fabrication process enabled many new structures that were previously not possible through the use of microwire technology (Kewley, Bower et al. 1997; Maynard, Hatsopoulos et al. 1999; Bragin, Hetke et al. 2000; Vetter, Williams et al. 2004; Johnson, Otto et al. 2005; Selim Suner 2005).

Some microfabricated probes are designed to mimic the previous generation of microwires, but yield increases in performance due to more consistent manufacturing strategies (Rousche and Normann 1998; Maynard, Hatsopoulos et al. 1999). While microfabricated probe processes enable a much larger design space for arrays to interface with the brain, they have been so far unsuccessful at exceeding the baseline performance of the microwires they were designed to replace (Williams, Rennaker et al. 1999; Schwartz 2004; Vetter, Williams et al. 2004; Polikov, Tresco et al. 2005; Otto, Johnson et al. 2006). Furthermore, the large cost associated with these devices has precluded wide scale adoption by many neuroscience researchers and clinicians.

III. Neural Probe Technology Application

Neural probe technology is typically used for extracting neuroelectrical

information from the brain (Ludwig, Uram et al. 2006). This data provides vital information for the understanding of neurophysiology, characterization of pathology, and generating output signals that can be used to control external prosthetic devices (Chapin, Moxon et al. 1999; Williams, Rennaker et al. 1999; Kennedy, Bakay et al. 2000; Wolpaw, Birbaumer et al. 2002; Anderson, Burdick et al. 2004; Schwartz 2004; Kipke, Shain et al. 2008; Digiovanna, Rattanatamrong et al. 2010). The structural characteristics of the brain, as studied anatomically or through imaging, yield valuable information about the expected function of the underlying neural system (Kotter and Wanke 2005). However, imaging and anatomical characterization lack the resolution and desired output metrics that are necessary to understand how the firing of individual neurons and ensembles combine to create sensory perception or even consciousness.

To better understand and interpret the neural firing patterns within the brain, new technological advances are required that incorporate the use of high channel counts that can simultaneously sample from large populations of neurons to yield more information about the underlying cortical morphology and structure. Many neural probe technologies exist that incorporate high numbers of electrode sites assembled from a large number of individual microwires (Ulbert, Halgren et al. 2001; Schwartz 2004). While these technologies achieve the throughput of information necessary for controlling external devices and brain-computer interfaces, they lack the ability to sample from a three-dimensional volume of neural tissue simultaneously (Rousche and Normann

1998; Lebedev and Nicolelis 2006; Ward, Rajdev et al. 2009). Other microfabricated structures can sample high channel counts and have been used in cortical mapping experiments, but these devices are only capable of sampling from a planar representation of the cortex (Csicsvari, Henze et al. 2003; Blanche, Spacek et al. 2005; Aarts, Neves et al. 2008; Du, Riedel-Kruse et al. 2009; Ludwig, Miriani et al. 2009; Ward, Rajdev et al. 2009). The simultaneous sampling of neural tissue in 3D enables mapping neural connections within the brain and understanding how these networks create sensory perceptions from firing of individual neurons. As the brain is not a two-dimensional structure, it is reasonable to assume that sampling from neural networks in three dimensions will be necessary to fully understand all the relevant interactions within the brain.

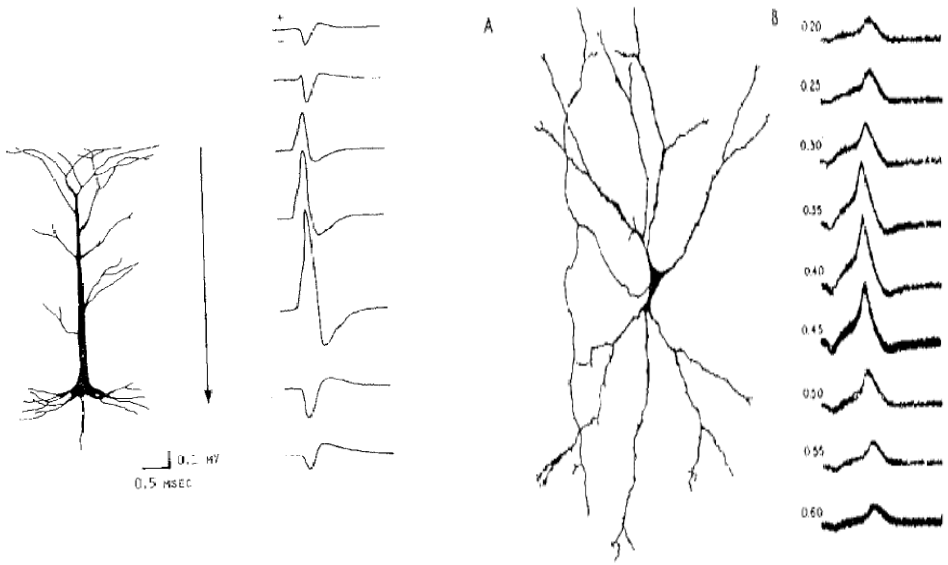

Figure I-2: Theoretical potential recorded as a microelectrode is driven past a pyramidal cell. (Right) Theoretical potential as a microelectrode is driven past a stellate cell. (Schmidt and Humphrey 1990)

IV. Electrode Modifications

A few groups have examined the use of conductive polymers, such as polypyrrole and Poly (3, 4-ethylenedioxythiophene polymer) (PEDOT), for the coating of neural recording probes (Cui, Lee et al. 2001; Cui, Wiler et al. 2003; Kim, Abidian et al. 2004). The primary motivation behind the modification of standard neural recording probes is to optimize the ability to record neural activity by decreasing the site impedance, which is typically larger on small silicon probes. By decreasing the impedance without greatly increasing the surface area, it may be possible to improve neural recording quality compared to that of standard iridium site probes (Ludwig, Uram et al. 2006). Many of the results of the previous studies are directly related to the reduction of electrode site impedance, which can be used in future probe designs utilizing small electrode sites.

V. Unit Detection and Spike Sorting

In order to understand extracellular neural recordings, one must first have a basic grasp of the original source of the recorded signal. As can be seen in Figure I-2, the recorded signal from a given neuron can be a function of the neural cell type, the orientation of the cell, and the location of the recording electrode relative to the fields generated by the neuron (Schmidt and Humphrey 1990). Given these variables, it may seem like a difficult problem to separate specific neurons from each other; however, a consistently positioned electrode should record a similar waveform shape each time a neuron fires (Strumwasser

1958; Burns, Stean et al. 1974; Liu, McCreery et al. 1999; Williams, Rennaker et al. 1999; Linderman, Gilja et al. 2006; Purcell, Seymour et al. 2009; Sharma, Rieth et al. 2010). There will always be some variability due to random noise sources added into the recordings, but these are assumed to have a fairly Gaussian shape (Lewicki 1998; Ludwig, Uram et al. 2006). Bursting neurons (neurons whose firing rate is substantially greater for brief periods) in response to a stimuli or as a part of neural circuit will in many cases have spike amplitudes that vary over successive action potentials. If a recorded waveform from the same neuron differs in shape between firings, these neurons will fail to be properly identified as being from the same source, independent of the system or algorithm used to discriminate them (Lewicki 1998). Using simultaneous intracellular recording of the same action potential, extracellular potentials have been correlated with individual spike responses (Henze, Borhegyi et al. 2000). Simultaneous intracellular recording is prohibitively difficult, so for this work, it is assumed that waveforms of a similar shape on a given channel arise from the same source and waveforms that change temporally may be classified incorrectly.

Detection of neural action potentials within a recording trace is typically accomplished through a threshold crossing process (Lewicki 1998). With user-directed techniques, a variable threshold line is ideally set such that the peaks of action potentials on a given channel cross the level, while background noise from neural as well as other sources do not. This decreases the amount of data that must be analyzed in subsequent processing steps. For automated

techniques, a more objective method is used whereby the threshold is calculated as a function of some attribute of the full wideband data trace. Frequent parameters are normally either a whole multiplier of the standard deviation, variance, or root mean square (RMS) of the signal, otherwise a reverse process may also be used such as a fraction of the peak positive or negative amplitude of the recordings (Lewicki 1998). While the latter is computationally simpler, motion artifact or large infrequent amplitude variation may prevent any signals from being selected out of the original trace. After the threshold crossing event has been determined, a preset number of samples, equivalent to 0.8 – 3 ms of data is extracted from the original trace to be further analyzed to determine whether the event arose from a separable neural action potential or a random perturbation.

For many manual sorting techniques, the processing could be complete at this point. Given a cumulative display of the waveforms, it is possible to select the units based solely on the amplitude and waveform characteristics of the extracted samples as compared to know neural action potential shapes (Lewicki 1998; Wood, Black et al. 2004). However, in cases where multiple neurons are recorded from the same electrode site, separation by amplitude methods can be impractical, if not impossible. To solve this problem, features of the waveform are calculated and used to help differentiate. Examples of features include, peak amplitude (positive or negative), peak or trough width, waveform duration, or principal components.

Principal components can describe most of the waveform characteristics and are used by many automated sorting algorithms. The idea behind principal component analysis (PCA) is to create a set of orthogonal vectors to capture the variability in a set of data, in this case, the shape of a recorded neural action potential. The principal components are calculated by determining the eigenvectors of the covariance matrix of the dataset. While it may take many orthogonal vectors to fully describe the dataset, much of the variability in the data is due to random fluctuations and competing noise sources. If the noise-dominated vectors are ignored, the first two or three principal components reconstruct a reasonable shape of the original action potential. For this reason, sorting techniques based on principal components typically examine the data in only 2 or 3 dimensions, which also simplifies visualization of the data (Lewicki 1998).

When examining a graphical representation of the principal components, data points from a given neuron typically cluster together in PCA space. The straightforward user-directed method for classifying these units as originating from a given neural source is referred to as cluster cutting. In this technique, technicians will circle all the data points that are in close proximity and group them together into a single cluster. While many experienced technicians employ this method, user-directed methods are frequently prone to classification errors (Wood, Black et al. 2004). Even in the best case scenario, this process can be fairly time consuming. Increasing channel counts further exacerbates this issue – assuming it take approximately 1 minute to analyze 1

channel of data, a 64 channel array would take over an hour to sort the data into given units. As the recorded waveforms may vary on a daily basis, this process becomes overly burdensome in any experiment that lasts more than a day.

To automate the process of clustering of waveforms, algorithms such as K-means or fuzzy c-means clustering are employed (Dunn 1974; Bezdek 1981). The basic process behind these techniques is to start with a given number of clusters of the data, generate random cluster centers, assign data points to the nearest cluster center, compute new cluster centers based on the member points, and iterate this process until a convergence criteria is met. In the case of fuzzy c-means clustering, the expectation maximization algorithm used to iterate the process is more statistically valid in the case of neural data as it includes partial membership into various clusters (Lewicki 1998). After clustering of the data is complete, the desired neural attributes can be selected from the processed data and used for either neurophysiological analysis or processing for another neuroprosthetic applications.

Given increasing numbers of channels in new electrode technologies, issues with user-directed processing of neural data can become even more problematic (Buzsaki 2004). For multidimensional neural probes to become commonplace, the techniques to analyze the data recorded in an automated and expedient way become even more important. For these reasons, this proposal is focused on ways to automate analysis of neural data, extract more

information from the data already recorded with existing probe technologies, using multi-core processors and distributed computing techniques to expedite analysis, and applying these techniques to the auditory brain system in a validation experiment using state of the art three dimensional neural probes.

VI. Dissertation Organization

This dissertation includes four studies which are either in press or preparation for submission to peer-review journals. The first chapter introduces the dissertation and provides relevant background information that is beyond the scope of the individual publications outlined in the middle chapters. The final chapter summarizes what has been completed in this thesis, the contribution to the field as a whole, and future directions for studies utilizing the work started here. All studies in this dissertation are focused on optimizing the information that can be extracted from cortical recordings using microelectrodes.

In Chapter 2, we developed automated techniques for extracting and clustering neural spikes utilizing standard MATLAB functions for principal component analysis and fuzzy c-means clustering. Since the future goal is to increase adoption of this technique through open source channels, we compared the performance of the MATLAB toolbox using recorded neural data with respect to current alternatives such as Offline Sorter (Plexon, Inc.), a commercially available neural data analysis package. We also used simulated data with known neural sources and timing to evaluate our toolbox with respect to the number of detected units, cluster location, number of clusters, and variability

between repeated iterations. Using these metrics, we have demonstrated that our package performs comparably to more expensive alternatives and is adaptable to multiple neural recording platforms as well as pseudo real-time analysis of high-density electrode arrays using clustered computing techniques. Chapter 2 is in preparation for submission to the *Journal of Neural Engineering*.

In Chapter 3, we introduce a technique to identify dendritic contributions to the potential recorded on distant electrode sites, providing additional information about the morphology of a recorded neuron in space with respect to the electrode array. To evaluate this technique, we implanted silicon microelectrode arrays in the motor cortex of Sprague Dawley rats and auditory cortex of guinea pigs. The site locations of the implanted microelectrode arrays enabled recording from multiple locations at multiple cortical depths simultaneously. The results of this study indicate that the potential fall off of a neuronal action potential is not analogous to homogenous fall off from a point source, but is instead influenced by neuronal morphology. Moreover, we demonstrated that the contribution of neuronal morphology to the extracellular potential can be detected by recording at precise locations dorsal to the site putatively recording from the cell body. Consequently, the methodology introduced here may enable more precise spike sorting techniques. Chapter 3 is in preparation to be published in *Journal of Neurophysiology* or *Journal of Neuroscience Methods*.

In Chapter 4, we investigated using poly(3,4-ethylenedioxythiophene) (PEDOT) to lower the impedance of small, gold recording electrodes with initial

impedances outside of the effective recording range. As expected, chronically implanted control electrodes were unable to record well-isolated unit activity, primarily as a result of a dramatically increased noise floor. Conversely, electrodes coated with PEDOT consistently recorded high-quality neural activity, and exhibited a much lower noise floor than controls. These results demonstrate that PEDOT coatings enable electrode designs of 15 microns in diameter. Chapter 4 has been recently accepted for publication in the *Journal of Neural Engineering*.

In Chapter 5, we present a proof of concept validation of a 3D probe technology consisting of 16 silicon shanks in a 4x4 grid arrangement with four electrode sites per shank. This 3D array has been implanted in guinea pig primary auditory cortex and electrophysiological data are presented showing the utility of electrode sites spanning multi-lateral cortical space as well as cortical depth. Using these devices, we were able to successfully map the tonotopic space with fewer insertions than would have been necessary with single wires or 2D probe architectures. Chapter 5 is in preparation for submission to *IEEE Transactions on Neural Systems and Rehabilitation Engineering*.

This dissertation provides several novel improvements to the current neuroprosthetic device, which have been evaluated in long-term chronic conditions. The results presented here not only impact the field of practical neuroprosthetic devices, but contributes to the fundamental understanding of microelectrode theory as a whole.

VII. References

Aarts, A. A., H. P. Neves, et al. (2008). "A 3D slim-base probe array for in vivo recorded neuron activity." Conf Proc IEEE Eng Med Biol Soc **2008**: 5798-5801.

Anderson, R. A., J. W. Burdick, et al. (2004). "Cognitive Neural Prosthetics." Science Direct **8**(11).

Bezdek, J. C. (1981). Pattern recognition with fuzzy objective function algorithms. New York, Plenum Press.

Blanche, T. J., M. A. Spacek, et al. (2005). "Polytrodes: high-density silicon electrode arrays for large-scale multiunit recording." J Neurophysiol **93**(5): 2987-3000.

Bragin, A., J. Hetke, et al. (2000). "Multiple site silicon-based probes for chronic recordings in freely moving rats: implantation, recording and histological verification." Journal of Neuroscience Methods **98**(1): 77-82.

Burns, B. D., J. P. Stean, et al. (1974). "Recording for several days from single cortical neurons in completely unrestrained cats." Electroencephalography and Clinical Neurophysiology **36**(3): 314-318.

Buzsaki, G. (2004). "Large-scale recording of neuronal ensembles." Nat Neurosci **7**(5): 446-451.

Chapin, J. K., K. A. Moxon, et al. (1999). "Real-time control of a robot arm using simultaneously recorded neurons in the motor cortex." Nat Neurosci **2**(7): 664-670.

Csicsvari, J., D. A. Henze, et al. (2003). "Massively parallel recording of unit and local field potentials with silicon-based electrodes." J Neurophysiol **90**(2): 1314-1323.

Cui, X., V. A. Lee, et al. (2001). "Surface modification of neural recording electrodes with conducting polymer/biomolecule blends." J Biomed Mater Res **56**(2): 261-272.

Cui, X., J. Wiler, et al. (2003). "In vivo studies of polypyrrole/peptide coated neural probes." Biomaterials **24**(5): 777-787.

Digiovanna, J., P. Rattanatamrong, et al. (2010). "Cyber-workstation for computational neuroscience." Front Neuroengineering **2**: 17.

Du, J., I. H. Riedel-Kruse, et al. (2009). "High-resolution three-dimensional extracellular recording of neuronal activity with microfabricated electrode arrays." J Neurophysiol **101**(3): 1671-1678.

Dunn, J. C. (1974). "A Fuzzy Relative of the ISODATA Process and Its Use in Detecting Compact Well Compact Well-separated Clusters." Journal of Cybernetics **3**: 32-57.

Gage, G. J., K. A. Ludwig, et al. (2005). "Naive coadaptive cortical control." J Neural Eng **2**(2): 52-63.

Henze, D. A., Z. Borhegyi, et al. (2000). "Intracellular features predicted by extracellular recordings in the hippocampus in vivo." J Neurophysiol **84**(1): 390-400.

Hochberg, L. R., M. D. Serruya, et al. (2006). "Neuronal ensemble control of prosthetic devices by a human with tetraplegia." Nature **442**(7099): 164.

Johnson, M. D., K. J. Otto, et al. (2005). "Repeated voltage biasing improves unit recordings by reducing resistive tissue impedances." Neural Systems and Rehabilitation Engineering, IEEE Transactions on [see also IEEE Trans. on Rehabilitation Engineering] **13**(2): 160-165.

Kennedy, P. R., R. A. Bakay, et al. (2000). "Direct control of a computer from the human central nervous system." IEEE Trans Rehabil Eng **8**(2): 198-202.

Kewley, D. T., J. M. Bower, et al. (1997). "Plasma-etched neural probes." Sensors and Actuators A: Physical **58**: 27-35.

Kim, D. H., M. Abidian, et al. (2004). "Conducting polymers grown in hydrogel scaffolds coated on neural prosthetic devices." J Biomed Mater Res A **71**(4): 577-585.

Kipke, D. R., W. Shain, et al. (2008). "Advanced neurotechnologies for chronic neural interfaces: new horizons and clinical opportunities." J Neurosci **28**(46): 11830-11838.

Kotter, R. and E. Wanke (2005). "Mapping brains without coordinates." Philos Trans R Soc Lond B Biol Sci **360**(1456): 751-766.

Lebedev, M. A. and M. A. Nicolelis (2006). "Brain-machine interfaces: past, present and future." Trends Neurosci **29**(9): 536-546.

Lewicki, M. S. (1998). "A review of methods for spike sorting: the detection and classification of neural action potentials." Network-Computation in Neural

Systems **9**(4): R53-R78.

Linderman, M. D., V. Gilja, et al. (2006). "Neural recording stability of chronic electrode arrays in freely behaving primates." Conf Proc IEEE Eng Med Biol Soc **1**: 4387-4391.

Liu, X., D. B. McCreery, et al. (1999). "Stability of the interface between neural tissue and chronically implanted intracortical microelectrodes." IEEE Trans Rehabil Eng **7**(3): 315-326.

Ludwig, K. A., R. M. Miriani, et al. (2009). "Using a common average reference to improve cortical neuron recordings from microelectrode arrays." J Neurophysiol **101**(3): 1679-1689.

Ludwig, K. A., J. D. Uram, et al. (2006). "Chronic neural recordings using silicon microelectrode arrays electrochemically deposited with a poly(3,4-ethylenedioxythiophene) (PEDOT) film." J Neural Eng **3**(1): 59-70.

Marg, E. and J. E. Adams (1967). "Indwelling multiple micro-electrodes in the brain." Electroencephalogr Clin Neurophysiol **23**(3): 277-280.

Maynard, E. M., N. G. Hatsopoulos, et al. (1999). "Neuronal interactions improve cortical population coding of movement direction." J Neurosci **19**(18): 8083-8093.

Olds, J., J. F. Disterhoft, et al. (1972). "Learning centers of rat brain mapped by measuring latencies of conditioned unit responses." J Neurophysiol **35**(2): 202-219.

Otto, K. J., M. D. Johnson, et al. (2006). "Voltage pulses change neural interface properties and improve unit recordings with chronically implanted microelectrodes." Biomedical Engineering, IEEE Transactions on **53**(2): 333-340.

Polikov, V. S., P. A. Tresco, et al. (2005). "Response of brain tissue to chronically implanted neural electrodes." J Neurosci Methods **148**(1): 1-18.

Purcell, E. K., J. P. Seymour, et al. (2009). "In vivo evaluation of a neural stem cell-seeded prosthesis." J Neural Eng **6**(2): 026005.

Rousche, P. J. and R. A. Normann (1998). "Chronic recording capability of the Utah Intracortical Electrode Array in cat sensory cortex." Journal of Neuroscience Methods **82**(1): 1-15.

Schmidt, E. and D. R. Humphrey (1990). Extracellular Single-unit Recording

Methods. Neurophysiological techniques. Clifton, N.J., Humana Press. **2:** 1-64.

Schwartz, A. B. (2004). "Cortical neural prosthetics." Annu Rev Neurosci **27**: 487-507.

Selim Suner, M. R. F., Carlos Vargas-Irwin, Kenji Nakata, and John P. Donoghue (2005). "Reliability of Signals from a Chronically Implanted, Silicon-based Electrode Array in Non-human Primate Primary Motor Cortex." Submitted to IEEE.

Sharma, A., L. Rieth, et al. (2010). "Long term in vitro stability of fully integrated wireless neural interfaces based on Utah slant electrode array." Appl Phys Lett **96**(7): 73702.

Strumwasser, F. (1958). "Long-Term Recording from Single Neurons in Brain of Unrestrained Mammals." Science **127**(3296): 469-470.

Ulbert, I., E. Halgren, et al. (2001). "Multiple microelectrode-recording system for human intracortical applications." J Neurosci Methods **106**(1): 69-79.

Vetter, R. J., J. C. Williams, et al. (2004). "Chronic neural recording using silicon-substrate microelectrode arrays implanted in cerebral cortex." IEEE transactions on bio-medical engineering **51**(6): 896-904.

Ward, M. P., P. Rajdev, et al. (2009). "Toward a comparison of microelectrodes for acute and chronic recordings." Brain Res **1282**: 183-200.

Williams, J., R. Rennaker, et al. (1999). "Long-term neural recording characteristics of wire microelectrode arrays implanted in cerebral cortex." Brain Res Brain Res Protocol **4**: 303–313.

Wolpaw, J. R., N. Birbaumer, et al. (2002). "Brain-computer interfaces for communication and control." Clin Neurophysiol **113**(6): 767-791.

Wood, F., M. J. Black, et al. (2004). "On the variability of manual spike sorting." Ieee Transactions on Biomedical Engineering **51**(6): 912-918.

Chapter II

Pseudo Real-Time Implementation of an Objective Method of Spike Extraction and Classification Package*

I. Abstract

High fidelity spike-based neural prostheses for brain computer interface applications require well isolated neural signals to be extracted from the brain using consistent and reliable automated methods. Commercially available solutions are capable of sophisticated analysis, but also carry a large financial cost. Data analysis technicians typically use principal components, waveform temporal characteristics, and amplitude features as metrics to represent signal characteristics. These technicians then determine if a voltage perturbation was caused by an action potential (commonly known as a "spike") or a noise source. Voltage perturbations deemed to be action potentials by the technician are then

* This article is in preparation. Authors: Nicholas B. Langhals, Kip A. Ludwig, TK Kozai, and Daryl R. Kipke.

assigned to an individual neuron or neural cluster. These techniques may be extremely variable due to the subjective sorting parameters leading to biases in the experimental analysis and the inability to compare data sets from different studies. Moreover, manual sorting is time consuming, and is not scalable to sorting neuronal units from high channel count electrode arrays.

There are a variety of commercially available software packages that provide many of the desired features for analysis of neural spike data. However, these tools are typically restricted to one neural recording platform, are high cost, and are not designed to handle high channel count data sets in pseudo-real time through the use of clustered computing techniques. Consequently, comparative studies between datasets from different subjects in different research groups using these tools are nearly impossible.

To address these issues, we developed automated techniques for extracting and clustering neural spikes utilizing standard MATLAB functions for principal component analysis and fuzzy c-means clustering. Since the future goal is to increase adoption of this technique through open source channels, we compared the performance of the MATLAB toolbox using recorded neural data with respect to current alternatives such as Offline Sorter (Plexon, Inc.), a commercially available neural data analysis package. We also used simulated data with known neural sources and timing to evaluate our toolbox with respect to the number of detected units, cluster location, number of clusters, and variability between repeated iterations. Using these metrics, we have

demonstrated that our package performs comparably to more expensive alternatives and is adaptable to multiple neural recording platforms as well as pseudo real-time analysis of high-density electrode arrays using clustered computing techniques.

II. INTRODUCTION

For decades, neuroscientists have been recording from individual microelectrodes implanted into the brain. These individual electrodes record, at most, a few action potentials (commonly called spikes, or units) from neurons surrounding the implanted electrode(Schmidt and Humphrey 1990). However, newly developed microfabricated electrode arrays and high channel count microwire assemblies facilitate recording more action potentials simultaneously from larger and more diverse regions of the brain(Schwartz 2004; Blanche, Spacek et al. 2005; Kipke, Shain et al. 2008). Brain computer interface systems for external control of external devices theoretically can take advantage of this additional information, but techniques for isolating large numbers of neural sources in a highly noisy environment are still in developmental stages(Gage, Ludwig et al. 2005; Lebedev and Nicolelis 2006).

The most common method of data analysis for neural spike information is through manual cluster cutting(Lewicki 1998). In this process, a user examines features of individual channels of neural data, such as the principal components, and circles a set of features to create units that most likely arise from an individual neural source. While many experienced technicians

exclusively use this procedure, user-directed methods are frequently prone to classification errors (Wood, Black et al. 2004). Even in the best-case scenario, this process can be time consuming and does not yield consistent metrics between data sets. Given the increasing numbers of channels available using newer electrode technologies, issues with user-directed processing of neural data can become even more problematic (Buzsaki 2004). By increasing the number of channels to manually analyze, analysis time grows unreasonably. Assuming it takes approximately 1 minute to analyze 1 channel of data, a 64 channel array would take over an hour to sort the data into individual units. As the recorded waveforms may vary on a daily basis, this process must be repeated for each session for every subject. Given that most researchers are working with multiple subjects over multiple days, the majority of their time can become consumed with just sorting the data.

In addition to higher channel counts on an individual array, separate electrode arrays are often implanted into different cortical locations simultaneously to study connections between different regions of the brain (Buzsaki 2004; Blanche, Spacek et al. 2005). This results in even more data that must be sorted and analyzed. Consequently, it is desirable to automate the process of extracting information from the recordings to alleviate the need for a user-directed analysis. By automating sorting, channels of data may be analyzed in parallel and datasets may be divided across multiple computer cores or even different systems altogether(Wood, Black et al. 2004).

Two of the major neural hardware manufacturers offer their own offline sorting packages. Tucker-Davis Technologies (TDT) offers "OpenSorter"; this package is designed to allow the user to classify individual spike snippets that have been recorded and saved to their tank format. While the package includes completely automated options for post-acquisition analysis of the data, the full sorting process cannot be completed post-hoc. The program currently does not allow the user to threshold wideband data to extract potential spike waveforms, meaning that sections of neural data which fail to cross the threshold are not stored for future analysis. Plexon Inc. offers a more feature-rich software package named "Offline Sorter". This software package satisfies some of the limitations of its TDT counterpart such as built in waveform extraction as well as multiple user configurable options and methods to use for spike sorting. However, this package contains many ways for the user to manipulate the outputs to fit desired responses, making objective comparisons between datasets and users potentially problematic. Moreover, “Opensorter” and “Offline Sorter” are not adaptable to other recording platforms, and cannot be easily implemented to handle large channel count datasets in pseudo real-time using clustered computer techniques, which limit their utility in comparing large data sets between labs using varying neural recording systems. Overall, the largest limitation of these packages is that the purchase price per license can make its use prohibitively difficult for new investigators with limited startup funds. The lack of a low-cost, open-source option makes data comparisons between research groups prohibitively difficult, slowing collaborative

advancement of neural probe technology.

For performance comparisons of multidimensional neural probes to become commonplace, techniques to analyze the data recorded in an automated, expedient, cost-efficient, and open-source way becomes even more important. For these reasons, we developed an automated MATLAB toolbox for analysis of neural data that is easily adaptable to all common neural recording platforms. This package has been utilized in multiple projects within our research group (Ludwig, Uram et al. 2006; Abidian, Ludwig et al. 2009; Langhals and Kipke 2009; Ludwig, Miriani et al. 2009; Purcell, Thompson et al. 2009; Rohatgi, Langhals et al. 2009). To validate the performance of our toolbox, we compared the performance of our toolbox to Plexon's "Offline Sorter" in analyzing neural data recorded from animal subjects. In addition, we tested the performance of our toolbox in analyzing simulated neural data, allowing us to quantify performance when the number of simulated neural sources and spike timings are known. This toolbox will be made available as an open source kit to assist with high-throughput data analysis for spike classification and quantification, and facilitate comparative performance analysis studies across research groups.

III. METHODS

A. *Neural Recordings*

All data used in this study were taken from previous experiments within the

research group(Langhals and Kipke 2009; Ludwig, Miriani et al. 2009). Sprague Dawley rats were implanted with electrodes in primary motor cortex. Neural recordings were acquired using a TDT multi-channel acquisition systems (RX5, Tucker-Davis Technologies, Alachua, FL) in an electrically and acoustically shielded booth. Neural electrophysiological recordings for all channels were fed through an anti-aliasing filter (0.35 Hz – 7.5 kHz) amplified, and sampled at ~25 kHz (RX5).

B. *Threshold Detection*

Neural recording segments were analyzed offline to determine the number of neurons recorded, noise levels, and signal amplitudes using this custom automated MATLAB (Mathworks Inc., MA) software. A amplitude threshold window was set 3.5 standard deviations above and below the mean of the sample distribution. For each peak exceeding the threshold window, a 2.4 ms candidate waveform snippet centered on the absolute minimum of the waveform was removed from the recorded segment and stored. The amplitude of the noise voltage for every recording site in each recorded segment was calculated after all candidate waveforms had been removed. Figure II-1 depicts a two second window of high speed neural data representative off the typical signal input into the sorting program.

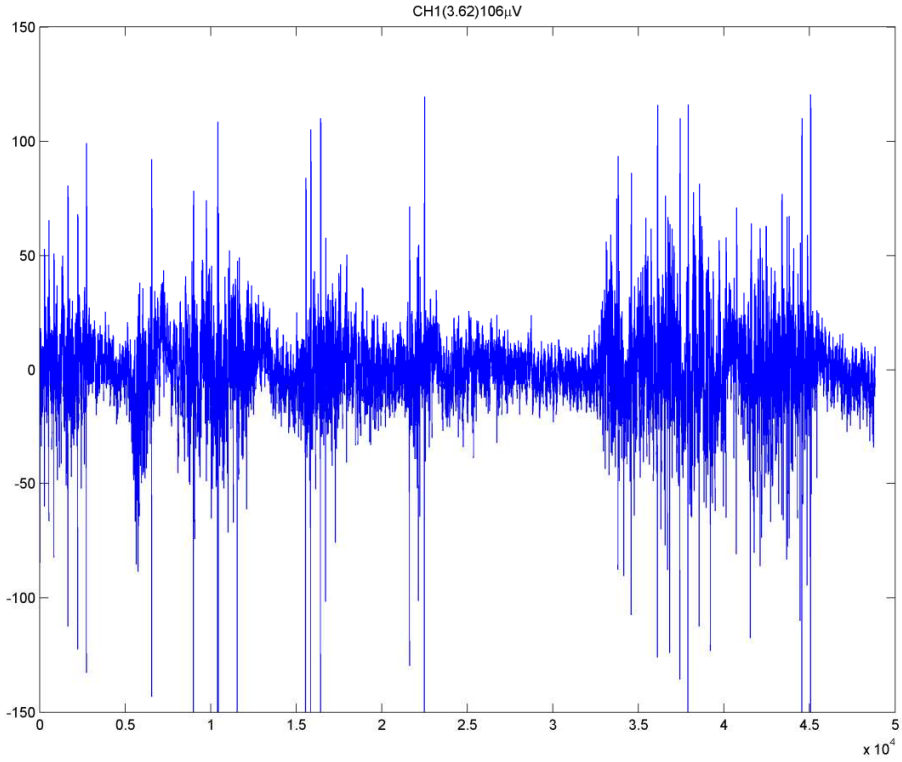

Figure II-1: Example plot showing high speed neural data/recordings input into the algorithm. The algorithm determined that the SNR of the mean waveform of the largest neuronal unit was 3.6 with a peak-peak amplitude of 106 μV. A low frequency oscillation is present on this channel; however the algorithm still successfully differentiated the signal from the noise.

C. *Clustering*

After initial principal component analysis, the first three principal components were plotted and analyzed in 3D space. Individual clusters were grouped and identified using fuzzy c-means clustering (Dunn 1974; Bezdek 1981; Ludwig, Uram et al. 2006). When compared to hard clustering, fuzzy clustering reduces classification errors resulting from the synchronous firing of multiple neurons (Zouridakis and Tam 2000). In order to determine the optimum number of clusters, the number of clusters was iteratively increased until the value for the

objective function calculated for k + 1 number of clusters was at least 55 percent of the value for the objective function calculated for k number of clusters (Karkkainen and Franti August 2002).

After clustering, waveforms with a cluster membership index of greater than 0.8 were used to determine a mean waveform for a cluster. Contributions of white noise and waveforms created by the simultaneous firing of multiple neurons generally do not have a membership index of greater than 0.8 for a particular cluster, and therefore were limited using this procedure (Zouridakis and Tam 2000). The toolbox then displays the principal components of all sorted waveforms. Unsorted waveforms can also be displayed if desired to visualize the separation of the units including ones that were excluded as arising from noise (Figure II-2).

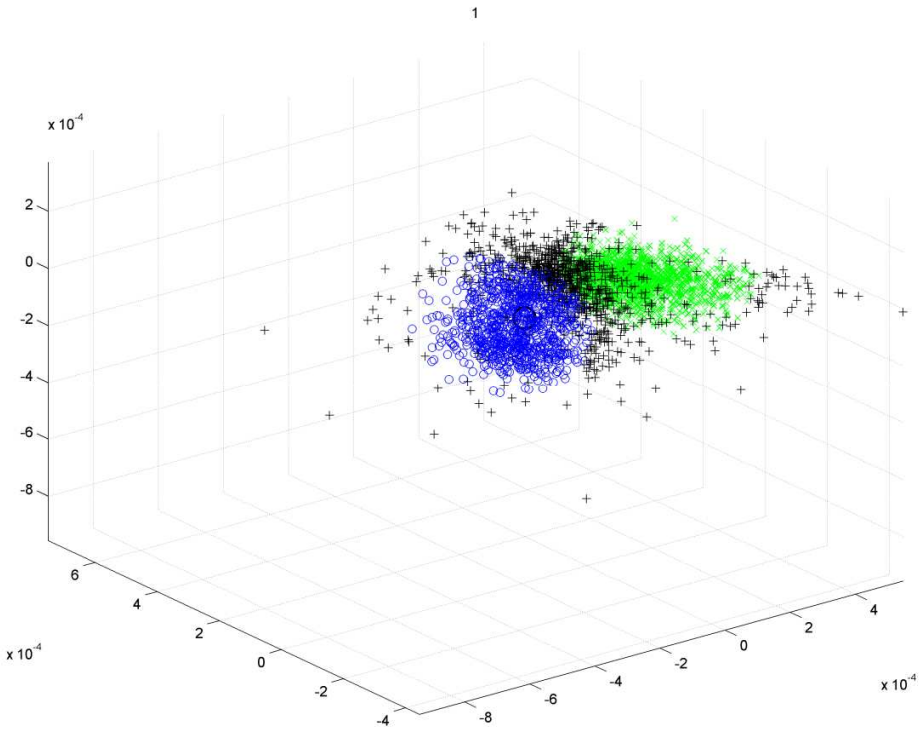

Figure II-2: Example cluster plot after sorting of the neural data. Blue and green symbols were separated by the algorithm as being more likely to arise from independent neural sources. Black symbols were insignificantly different and therefore were left unsorted by the algorithm.

D. *Sorted Waveform Characteristics*

Signal amplitude for a cluster was defined as the peak-to-peak amplitude of the mean waveform for each cluster. The signal-to-noise ratio (SNR) for a given cluster was defined as the Signal Amplitude / (Peak-to-Peak Amplitude of the Noise Floor).

The peak-to-peak amplitude of the noise on a given site was calculated as six times the standard deviation of the recording after waveforms that exceeded threshold were removed, spanning approximately 99.7 percent of normally

distributed noise data (Blanche, Spacek et al. 2005). By using this method, the calculated signal-to-noise ratio and peak-to-peak noise amplitude on a given site was more consistent with a visual inspection of the recorded voltage traces. For example, an SNR of 2 would indicate that the mean peak-to-peak amplitude of the signal was twice as large as the peak-to-peak amplitude of the noise floor. As the peak-to-peak amplitude of the noise floor for neural recordings is typically between six and ten times larger than the root mean square (RMS) value of the noise floor (Blanche, Spacek et al. 2005), SNR calculations for neural recordings based on the RMS of the noise floor raise the SNR with respect to peak-to-peak values.

Clusters with a mean SNR of 1.1 or greater were considered discriminable units, as the signal amplitude of these clusters was sufficient to be reliably differentiated from the noise floor (See Figure II-1). Conversely, clusters generated by random outlying perturbations from sources of noise had mean SNR values of 0.9 or less. Although normally distributed noise sources will occasionally exceed the 3.5 standard deviation threshold by random chance, the average waveform generated by these noise sources returns to zero after crossing threshold (instead of exhibiting an immediate opposing peak). Consequently, the mean waveform of a noise cluster spans less than six standard deviations of the noise floor, resulting in a calculated SNR of less than 1. When adjusted for the difference between calculating SNR using peak-to-peak amplitude of the noise floor instead of RMS, an SNR of 1.1 or greater corresponded well with observations of ‘moderate or better’ unit quality based

on SNR values from similar recording studies (Henze, Borhegyi et al. 2000; Suner, Fellows et al. 2005; Ludwig, Uram et al. 2006). Figure II-3 depicts example output from the toolbox, including sorted waveforms and mean waveform shapes.).

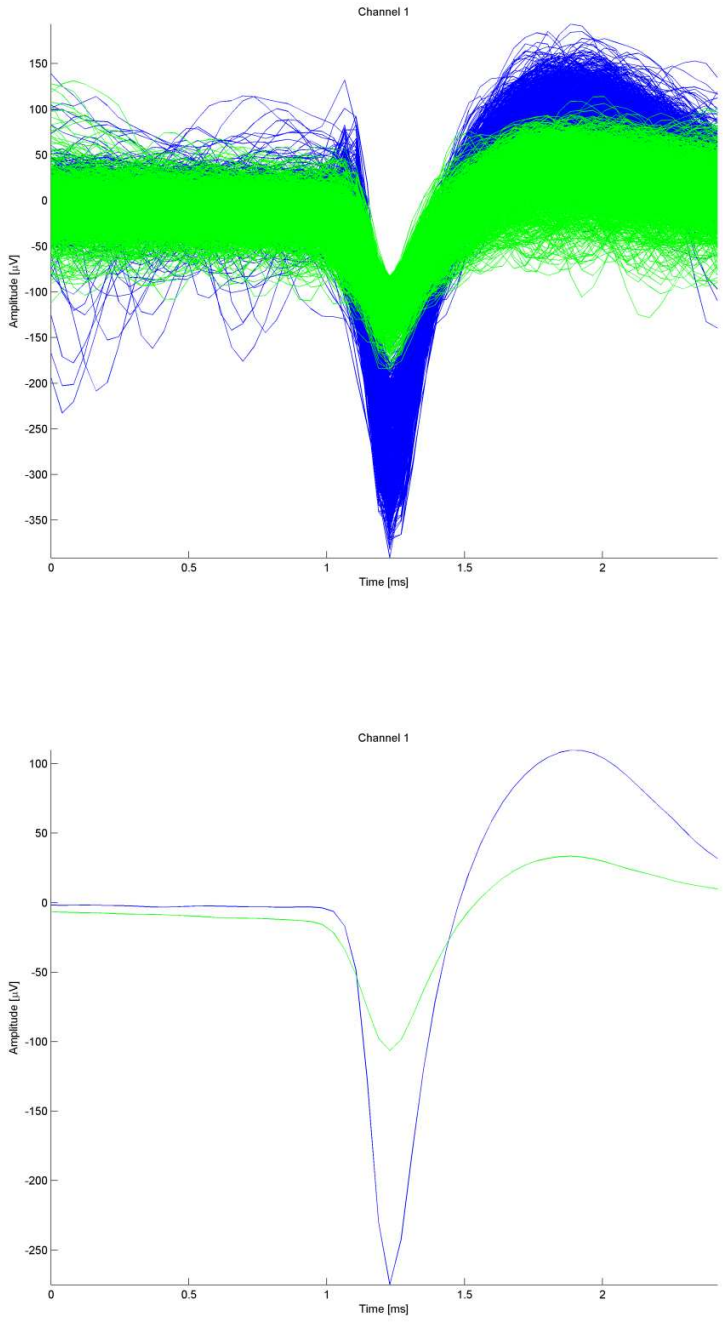

Figure II-3: Two distinct neural sources extracted from the data in previous figures. The blue trace has an SNR of 3.6, while the SNR of the green channel is 1.3. While the smaller channel is not as well isolated, the algorithm was still able to extract it from the noisy traces in Figure II-1.

E. *Autocorrelogram*

In order to verify that individual sorted units are likely to arise from an individual neuron, an autocorrelogram or an inter-spike interval histogram must be calculated. To do this, all waveform time stamps were aggregated and the times between each of the firing of the unit are plotted(Lewicki 1998). As neurons have an absolute refractory period wherein a neuron cannot generate an action potential immediately after firing due to sodium channel inactivation, a low number of spike counts should be evident near zero (Henze, Borhegyi et al. 2000). Neurons also have a relative refractory period after generating an action potential wherein some of the channels are still inactivated, resulting in a lower probability of generating an additional action potential for a few more milliseconds(Lewicki 1998). The autocorrelogram of a well isolated neuron should therefore consist of a plus or minus 2 ms period centered at time 0 (the time of the first action potential) where there are no additional spike counts generated by the neuron due to the absolute refractory period. Similarly, during the period plus or minus 2-10 ms from time 0, there should be fewer spike counts due to the relative refractory period. Consequently, the negative space of an autocorrelogram from a well-isolated neuron resembles a “V”. This toolbox also plots the autocorrelogram to verify this information visually (Figure II-4).

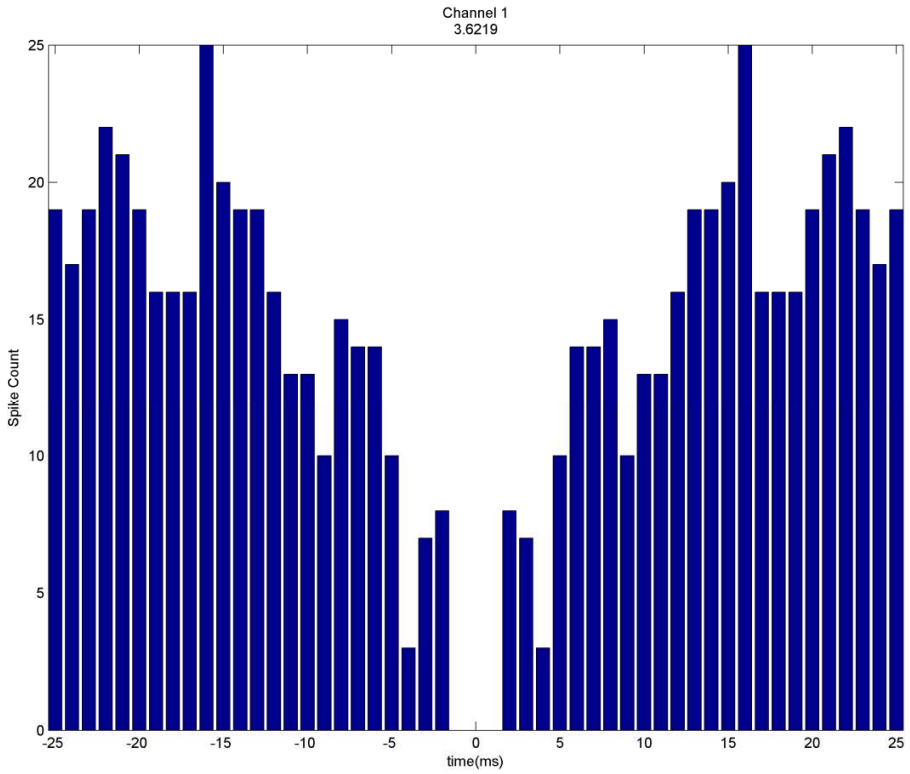

Figure II-4: Autocorrelogram of the blue waveform in previous figures. Ideally, there should be no spike counts 0-2 ms before or following a spike (t=0 ms), indicative of the absolute refractory period as seen above. Moreover, there should be fewer spike counts in the periods 2-10 ms before or after a spike, indicative of the relative refractory period. Jitter in the plot is due to variations in spike shape, false negative classifications, and noise sources within the neural recordings.

F. *Offline Sorter Comparison*

For performance comparisons between Offline Sorter and the MATLAB toolbox, consistent Offline Sorter settings were selected to as closely match the options in our toolbox as possible. Data recorded from rat cortical neurons in prior experiments was processed through both our MATLAB algorithm as well as Offline Sorter. After data format conversion, the wide-band data was loaded into Offline Sorter. A 300 Hz high-pass filter was applied to the neural data to

remove local field potentials from further analysis. A threshold for spike detection was set at 3.5 standard deviations and a 2.4 ms window was extracted from the data for each individual waveform. The window was set such that 1/2 of the window duration was pre-threshold and the remainder was post-threshold. All waveforms were then aligned in the program so that the negative peaks were at the same location to decrease variability in the principal components. Both automated sorting options in the program, Valley Seeking & T Distribution E-M, were tested for comparison. Ultimately E-M sorting was used for all further analyses as it is most comparable to the sorting technique presented in this paper.

G. *Simulated Data*

For quantitative analysis of the functionality of our algorithm, simulated data was generated with known spike locations for analysis. This data was developed with assistance from collaborators and used in their testing of onboard processing for neural spike sorting applications. Simulated spikes were generated of various SNR's ranging from 0 dB to 18 dB. The SNR of the simulated data was defined differently than that of the output of the algorithm. To create the data, an SNR was defined as $20 * \log_{10} (SD_{signal}/SD_{noise})$. Noise data was selected from previous recording sessions in which no neural sources were visible and a random Gaussian noise was added to the input spike signal for variability. The spike signal was composed of 3 out of 10 possible spike waveforms randomly placed throughout the data file (Figure II-5). Spike

waveforms were normalized such that the peak value (either positive or negative) was defined as 1. Given this definition, not all waveforms on a given channel have the same peak-to-peak amplitude (Table II-2). Noise on a given channel was varied to generate simulated neural sources with differing signal to noise ratios. Ten channels of data were tested per file so that all possible waveforms were examined. The data files that resulted from this methodology included waveforms with variations around a defined SNR value. For example, at 0 dB, all waveforms had a net spike SNR of at most 1.0. At 5 dB, the mean SNR across channels increased to 1.4, and the largest value of 18 dB lead to easily detectable units with SNRs over 4.0 (Table II-2).

Table II-1: Spike Amplitude and SNR levels for Simulated data files. SNR for each channel is defined as the peak to peak amplitude of the spike template divided by the noise level in the recording session. Noise level was calculated as 6 times the standard deviation to coincide with the SNR calculations by the algorithm. The channel on which each waveform spike is present is indicated in the header row. For example, Channel 1 contains spike templates 1, 2, & 3.

Spike Template (Channels)	**1 (1,7,8)**	**2 (1,2,8)**	**3 (1,2,10)**	**4 (2,3,9)**	**5 (3,4,10)**	**6 (3,4,5)**	**7 (4,5,6)**	**8 (5,6,9)**	**9 (6,7,10)**	**10 (7,8,9)**
Spike V_{pp}	1.7	1.1	1.4	1.6	1.8	1.5	1.9	1.1	1.6	1.2
0 dB SNR (1.92 Noise)	0.9	0.6	0.7	0.8	0.9	0.8	1.0	0.55	0.8	0.6
5 dB SNR (1.07 Noise)	1.6	1.0	1.3	1.5	1.6	1.4	1.8	1.0	1.4	1.1
18 dB SNR (0.26 Noise)	6.6	4.1	5.3	6.2	6.8	5.6	7.4	4.1	6.0	4.6

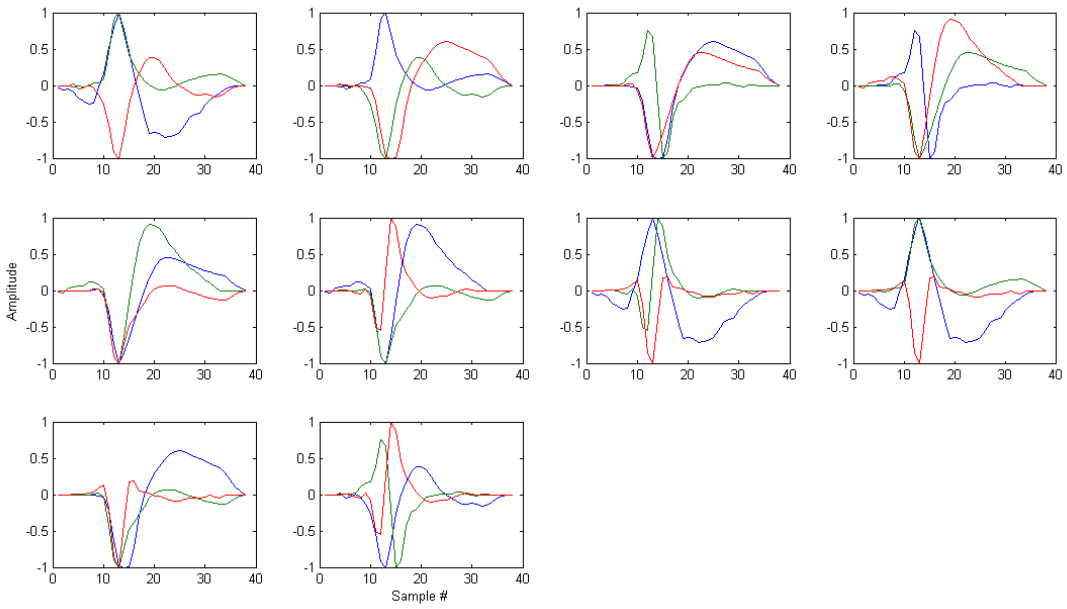

Figure II-5: Spike waveforms used for each channel of simulated data. Three waveforms were used in each channel of different shapes to examine the algorithm's ability to separate similar shaped waveforms of differing amplitudes.

IV. RESULTS/DISCUSSION

A. *Comparison to OFS*

Our MATLAB sorting toolbox was first compared to Offline Sorter using a single channel of neural data recorded in a prior experiment. The same dataset as used above (Figure II-1, Figure II-2, Figure II-3, Figure II-4) was exported from the TDT software environment into a format that is compatible with Offline Sorter (.DDT file) using a modified version of OpenBrowser provided to the authors by TDT. The data was filtered, waveforms snippets over the threshold were extracted and the principal components were clustered in 3D space as described in the methods. Both Offline Sorter and our toolbox isolated two units

with almost identical mean waveforms (Figure II-6 and Figure II-3, respectively). However, Offline Sorter also created an additional waveform cluster from the remaining data that our MATLAB toolbox eliminated. Note that this additional waveform resembles random noise that incidentally crossed the threshold (a singular low amplitude negative voltage deflection that immediately returns to zero), and is therefore either very low amplitude neural hash that is impossible to differentiate from noise, or simply noise.

The number of detected waveforms and other cluster characteristics were then compared between the two software packages. Offline Sorter detected a total of 7553 waveforms of which 772 were classified in the blue unit and 2120 were classified in the green unit. In contrast, the MATLAB package detected 3329 threshold crossings and classified 839 in the blue unit and 1575 in the green unit. Note that both Offline Sorter and our toolbox detected a similar number of detected waveforms for the blue unit.

The discrepancy in the number of waveforms results from multiple sources. As noted above Offline Sorter's unit "a" (yellow) is simply random noise that was of sufficient amplitude to cross the threshold level. Offline Sorter normally assigns any clustered points to an additional unit, even if they are low SNR, whereas our algorithm excludes them appropriately as noise. Small differences in the number of blue units detected are likely due to differing classification between the edges of the clusters as the blue and green units begin to overlap. Our toolbox also detected considerably fewer green units than Offline Sorter. Note

that many of the green units detected by Offline Sorter overlap in cluster space with yellow units generated by noise. As the true number of underlying sources is not known in recorded neural data, it is impossible to tell if these are true units or noise perturbations. Offline Sorter's arbitrary sorting method results in clusters where noise is occasionally classified as units. In contrast, our toolbox has been designed conservatively, and is therefore unlikely to classify noise as a unit. There is always a tradeoff between false positives and false negatives, so we have chosen to exclude some potentially useful information in neural hash / multi-unit activity at the expense of being able to exclude more of the noise. For evaluating improvements in neural probe technology, one would prefer fewer false positives and will accept additional false negatives to be confident that all neural sources detected are real.

Other quantitative comparisons of metrics were impossible as Offline Sorter does not have options to calculate noise level in the wideband data, peak-to-peak signal level, spike rate, etc. Furthermore, as a scale factor of 1 million was used in OpenBrowser to convert from floating point data to integer Offline Sorter data, all amplitudes listed in the Offline Sorter package are not indicative of the original recorded amplitude. In summary, both the MATLAB toolbox and Offline Sorter created similar mean waveforms for 2 units, with similar unit counts adjusting for slight differences in methodology such as stricter cluster criteria. Our MATLAB toolbox excluded the 3rd unit created by Offline Sorter, which appears to be either entirely noise, or multi-unit hash that is not differentiable from noise.

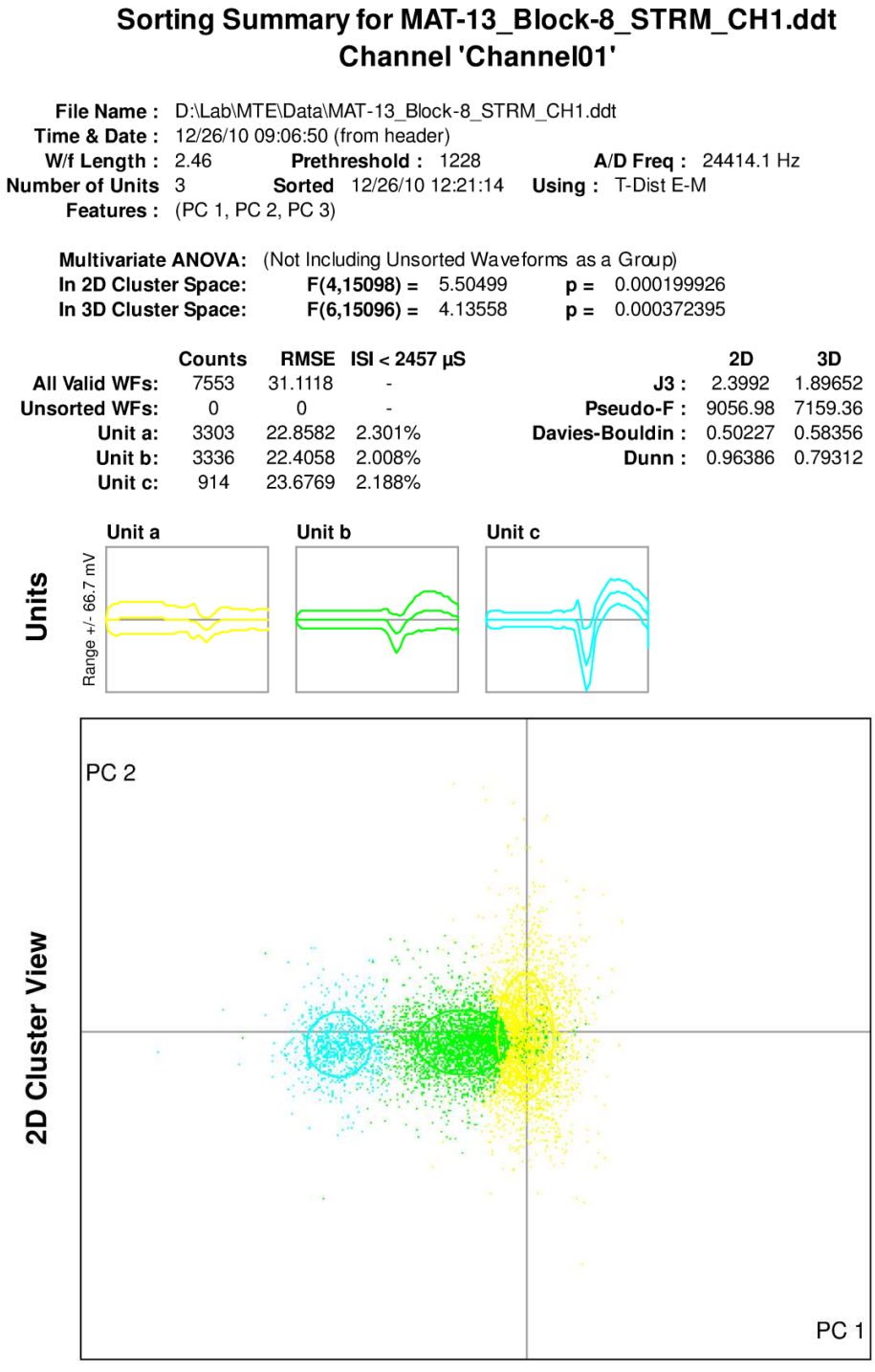

Figure II-6: Sorting Summary for single channel data processed using Offline Sorter. Blue and Green units are representative of similar data as in Figure II-3.

B. *Simulated Data in MATLAB*

To better characterize the efficacy of the MATLAB package, we analyzed a set of simulated neural data with known neural sources. The dataset had ten channels with three spike waveforms per channel for signal added to a combination of Gaussian noise and real neural noise. We varied the SNR of the simulated data to analyze the efficacy of spike detection in emulated practical recording situations (Table II-2). As can be seen in Table II-2, our algorithm successfully detected the majority of input waveforms correctly and performed with greater than 97% accuracy across all waveform shapes in the 18 dB high SNR situations. The few waveforms that were not correctly clustered were near the edges of the clusters as can be seen by the unsorted black units in the upper plot of Figure II-7. These waveforms had membership indexes that were not quite high enough to be included in the cluster, likely due to the close proximity to neighboring clusters. There was also increased jitter in waveform shape resulting from simulated noise.

Waveforms were selected for each channel such that similar waveforms as well as individually distinct waveforms were combined on the same channels. On channel 3, two waveforms with extremely similar waveform shapes were both selected to examine how well the algorithm performed with overly similar characteristics (See Figure II-5). These two waveforms did not have the sufficiently differentiable principal components to be separable as is evident in the upper cluster plot (Figure II-7). Moreover, even experienced technicians

would likely group these clusters together under the assumption that the slight separation between them was due to random perturbations in the neural environment as opposed to arising from different neurons.

Table II-2: Simulated spike data. Total number of waveforms and accuracy for successful detection and sorting are displayed.

Channel	Total Waveforms Input to Algorithm	Total Waveforms Detected at 18dB	Algorithm Accuracy per Channel
1	2088	2083	99.8%
2	2007	2007	100%
3	1702	1702	100%
4	1487	1486	99.9%
5	1553	1523	98.1%
6	1710	1671	97.7%
7	1780	1749	98.3%
8	1974	1965	99.5%
9	1677	1634	97.4%
10	1560	1560	100%

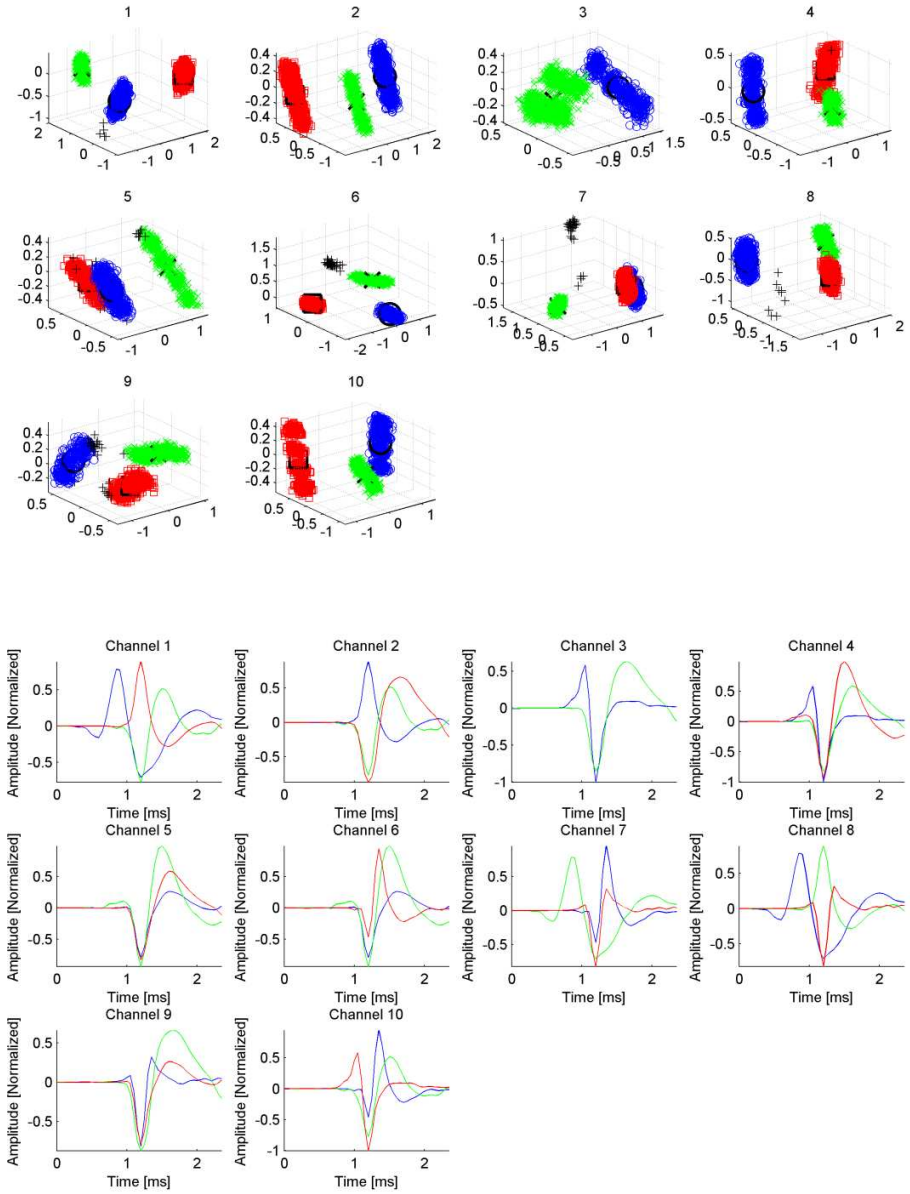

Figure II-7: Waveforms detected from simulated data with the largest tested SNR of 18 dB. Upper plot is clusters of principal components. Greater than 97% of waveforms in the input to the algorithm were successfully detected on every channel. In one case on channel 3, 100% of the waveforms were detected and clustered, however two of the waveforms were similar enough to be classified as a single green unit. Given this extremely similar shape of the waveforms as seen in Figure II-5, it was expected that these would likely be clustered together.

In the dataset for the channel used in the simulated data comparison, there were 840 presentations of unit 1(blue-1.6), 460 of unit 2 (green-1.3), and 788 of unit 3 (red-1.0).

To examine the functionality of our algorithm when given recordings consisting of low amplitude signal and a high noise floor we used an simulated SNR signal of 5 dB, which produced spike SNR recordings near the minimum classifiable level of 1.1. When the simulated spike had an SNR of 1.0, 100% of the 788 waveforms were successfully detected and classified, though there were an additional 8% false positives due to high noise and waveforms similarities. For the other SNR levels of 1.3 and 1.6, an increase in the number of detected, but unsorted waveforms becomes visible (Figure II-8). For the 1.3 SNR unit, 57% of the 460 were correctly classified, compared to 41% of the 840 for the 1.6 SNR unit This increase in detected, but unclassified waveforms is due to the variability in waveform shape from the addition of the noise into the input simulated data. As the noise is added to the signal, random noise levels can substantially adjust waveform shape, as is typical in real cortical recordings. Even at this increased noise level, over two thirds of the total waveforms were successfully classified indicating that our algorithm performs in an acceptable and consistently objective manner, while providing a conservative estimate of number of units detected.

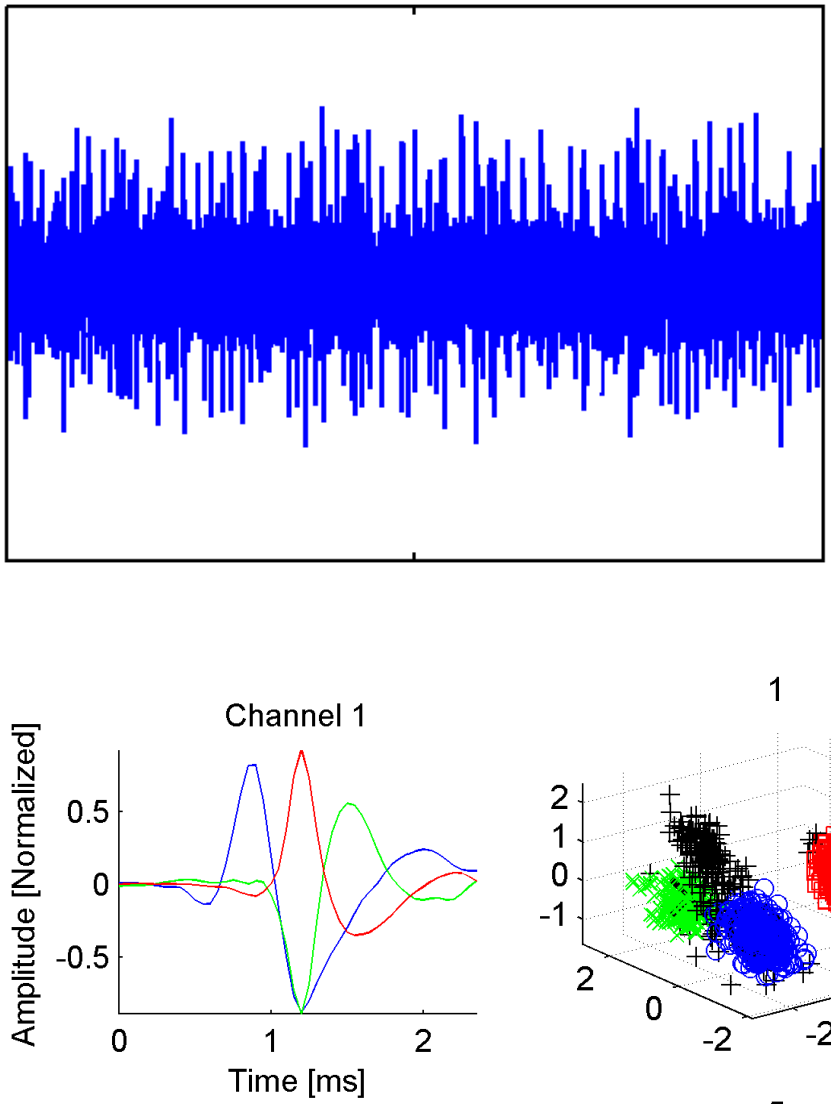

Figure II-8: Example higher noise data at a 5 dB simulated level. Upper plot shows an example two second signal input to the algorithm with all 3 waveforms. All three waveforms are correctly detected on the channel. These three waveforms have SNRs of 1.6, 1.3, and 1.1. Even at these lower SNR levels, 70% of the waveforms were correctly classified with 99% of the 1.6 SNR being identified perfectly. Black (+) clusters were detected however, the increased noise level made statistically significant differentiation less confident, resulting in an increase in unclassified waveforms.

C. *Comparison of Simulated Data Analyzed with Offline Sorter*

The same dataset described above was then converted and analyzed using Offline sorter for direct comparisons to be determined. For the high noise

dataset, Offline Sorter successfully detected an classified 54% of the waveforms overall (Figure II-9). For the waveforms with a 1.3 SNR, 100% of the 460 waveforms were classified correctly, along with 9 additional false positives. However, for the 1.6 and 1.0 SNR, Offline Sorter correctly classified 50% and 32% of the waveforms correctly respectively. Comparing these results to the same data processed using the MATLAB toolbox, one unit was completely classified in both packages along with some false positives. In high noise recordings such as those used in this simulated data session, false positive waveforms are substantially more likely as noise waveforms begin to approximate noisy spike waveforms. For the additional two waveforms, both detection and clustering efficiency are similar between the packages, however ours has a net higher performance of 67% over the 54% of Offline Sorter. This performance increase is primarily due to our threshold technique, which allows setting of positive and negative thresholds whereas Offline Sorter includes only one direction - allowing some waveforms to be undetected.

In low noise recording sessions, both packages perform similarly well. Offline Sorter detected and clustered 100% of the 1.3 SNR unit correctly along with 92% of the 840 waveforms in 1.6 SNR unit. However, for the 1.0 SNR unit all waveforms were clustered of the 778 possible along with an additional 9% false positives. All of these false positives should have been identified as the 1.6 SNR unit but were incorrectly classified into 1.0 unit resulting in an overall performance of 100% units classified with 8% incorrectly and an additional 1% false positive noise included.

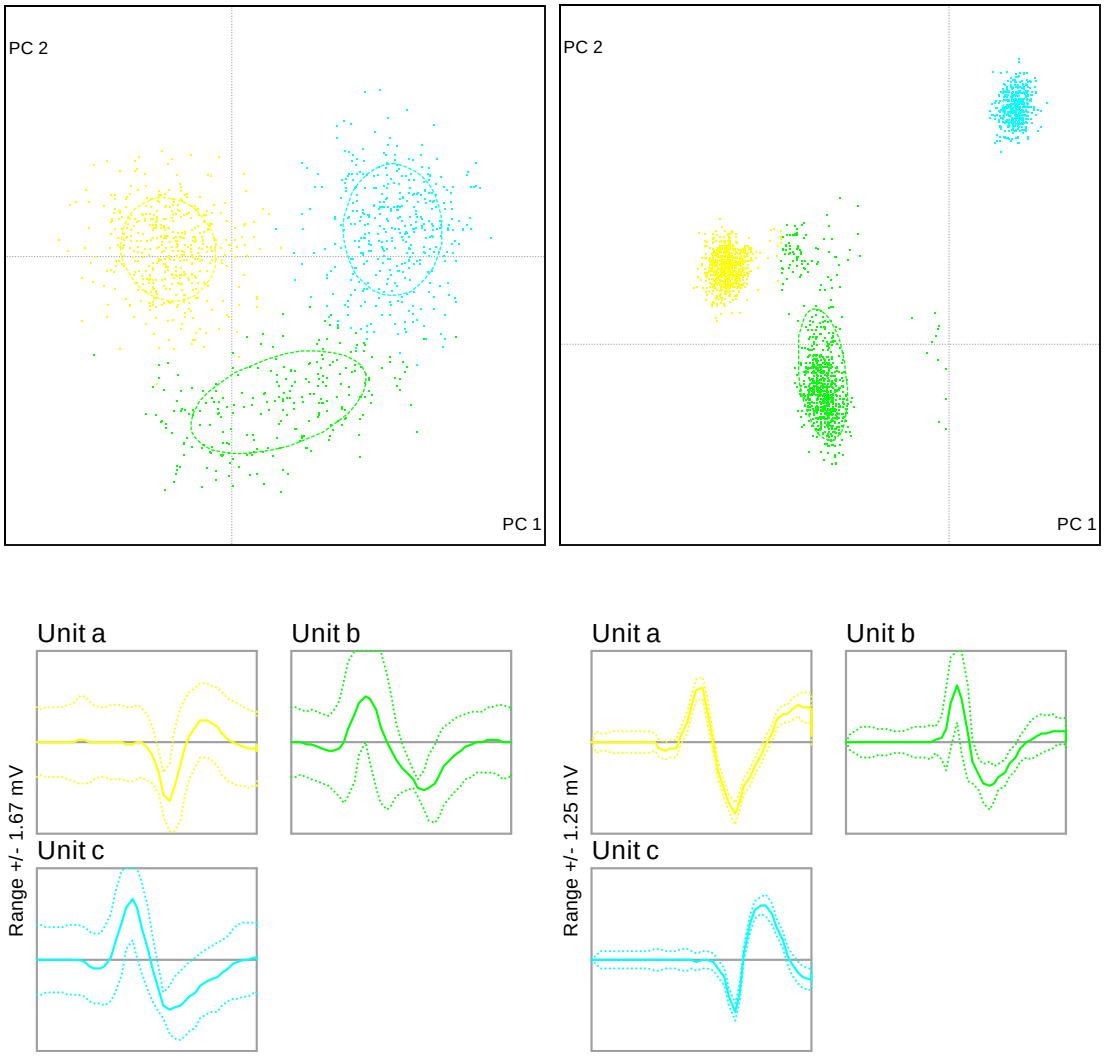

Figure II-9: Simulated Data processed using Offline Sorter. Left plots represent high noise simulated data while right plots represent the low noise situation. Upper plots are 2D cluster representations and lower plots are mean waveforms with waveform variability for each of the sorted units.

V. CONCLUSIONS

Within this study, we have developed and reported an automated MATLAB toolbox for analysis of neural data that is easily manipulated based on the experimental paradigm. This package has been utilized in multiple projects within our research group (Ludwig, Uram et al. 2006; Abidian, Ludwig et al.

2009; Langhals and Kipke 2009; Ludwig, Miriani et al. 2009; Purcell, Thompson et al. 2009; Rohatgi, Langhals et al. 2009). The algorithm package analyzes large amounts data quickly, provides objective classification of neural data across multiple platforms, and is open-source and therefore available at substantially reduced cost when compared to commercially available products. Our algorithm outperformed Offline Sorter while using well-isolated simulated data in a low noise recording session by correctly identifying 99.8% of the simulated units, where Offline Sorter misclassified 8% of units into the wrong cluster and incorporated 1% false positive events from noise into the results.

To expedite development and characterization of new neural probe designs and modifications, it is necessary for different researchers and developers to have a consistent standard for comparing device performance. Given the purchase price and limited adaptability of commercial packages, the most efficient way to accomplish this is through a collaborative open source neural data analysis package. We have successfully taken the first step towards this goal with the validation of this toolbox within our own research group. Furthermore, we have recently recruited beta testers who utilize both TDT and Plexon neural recording platforms to verify the basic functionality of the toolbox. After the currently running phase of beta testing, the toolbox will be available as an open source kit for use in research environments to assist with high throughput neural recording data analysis.

VI. ACKNOWLEDGEMENTS

The authors would like to thank Dr. Awais Kamboh & Dr. Andrew Mason from Michigan State University for assistance with providing simulated data and all of the members of the Neural Engineering Laboratory at the University of Michigan for their assistance in this study.

VII. GRANTS

This work was supported by the NIH P41 Center for Neural Communication Technology (EB002030) and the Whitaker Foundation.

VIII. DISCLOSURES

Daryl R. Kipke has significant financial interest in NeuroNexus Technologies, a leading supplier of microelectrode technology. Nicholas B. Langhals was a consultant for NeuroNexus Technologies.

IX. REFERENCES

Abidian, M. R., K. A. Ludwig, et al. (2009). "Interfacing Conducting Polymer Nanotubes with the Central Nervous System: Chronic Neural Recording using Poly(3,4-ethylenedioxythiophene) Nanotubes." Advanced Materials **21**(37): 8.

Bezdek, J. C. (1981). Pattern recognition with fuzzy objective function algorithms. New York, Plenum Press.

Blanche, T. J., M. A. Spacek, et al. (2005). "Polytrodes: High-Density Silicon Electrode Arrays for Large-Scale Multiunit Recording." J Neurophysiol **93**(5): 2987-3000.

Buzsaki, G. (2004). "Large-scale recording of neuronal ensembles." Nat Neurosci **7**(5): 446-451.

Dunn, J. C. (1974). "A Fuzzy Relative of the ISODATA Process and Its Use in Detecting Compact Well Compact Well-separated Clusters." Journal of Cybernetics **3**: 32-57.

Gage, G. J., K. A. Ludwig, et al. (2005). "Naive coadaptive cortical control." J Neural Eng **2**(2): 52-63.

Henze, D. A., Z. Borhegyi, et al. (2000). "Intracellular features predicted by extracellular recordings in the hippocampus in vivo." J Neurophysiol **84**(1): 390-400.

Karkkainen, I. and P. Franti (August 2002). Dynamic Local Search for Clustering with Unknown Number of Clusters. Int. Conf. on Pattern Recognition, Quebec, Canada.

Kipke, D. R., W. Shain, et al. (2008). "Advanced neurotechnologies for chronic neural interfaces: new horizons and clinical opportunities." J Neurosci **28**(46): 11830-11838.

Langhals, N. B. and D. R. Kipke (2009). "Validation of a novel three-dimensional electrode array within auditory cortex." Conf Proc IEEE Eng Med Biol Soc **2009**: 2066-2069.

Lebedev, M. A. and M. A. L. Nicolelis (2006). "Brain-machine interfaces: past, present and future." Trends in Neurosciences **29**(9): 536-546.

Lewicki, M. S. (1998). "A review of methods for spike sorting: the detection and classification of neural action potentials." Network-Computation in Neural Systems **9**(4): R53-R78.

Ludwig, K. A., R. M. Miriani, et al. (2009). "Using a common average reference to improve cortical neuron recordings from microelectrode arrays." J Neurophysiol **101**(3): 1679-1689.

Ludwig, K. A., J. D. Uram, et al. (2006). "Chronic neural recordings using silicon microelectrode arrays electrochemically deposited with a poly(3,4-ethylenedioxythiophene) (PEDOT) film." J Neural Eng **3**(1): 59-70.

Purcell, E. K., D. E. Thompson, et al. (2009). "Flavopiridol reduces the impedance of neural prostheses in vivo without affecting recording quality." J Neurosci Methods **183**(2): 149-157.

Rohatgi, P., N. B. Langhals, et al. (2009). "In vivo performance of a

microelectrode neural probe with integrated drug delivery." Neurosurg Focus **27**(1): E8.

Schmidt, E. and D. R. Humphrey (1990). Extracellular Single-unit Recording Methods. Neurophysiological techniques. Clifton, N.J., Humana Press. **2:** 1-64.

Schwartz, A. B. (2004). "Cortical neural prosthetics." Annu Rev Neurosci **27**: 487-507.

Suner, S., M. R. Fellows, et al. (2005). "Reliability of signals from a chronically implanted, silicon-based electrode array in non-human primate primary motor cortex." Neural Systems and Rehabilitation Engineering, IEEE Transactions on [see also IEEE Trans. on Rehabilitation Engineering] **13**(4): 524-541.

Wood, F., M. J. Black, et al. (2004). "On the variability of manual spike sorting." Ieee Transactions on Biomedical Engineering **51**(6): 912-918.

Zouridakis, G. and D. C. Tam (2000). "Identification of reliable spike templates in multi-unit extracellular recordings using fuzzy clustering." Computer Methods and Programs in Biomedicine **61**(2): 91-98.

Chapter III

Spike Triggered Averaging of Neural Recordings to Aid In-Vivo Visualization of Neuronal Morphology*

In standard chronic single-unit neural recordings, one or more electrodes are used to record the extracellular potential generated by an individual neuron. Although spike sorting methods are sufficient to isolate individual specific neurons, they do not yield information about the underlying morphology of the recorded neuron. Because the potential field generated by a firing neuron falls off quickly with respect to distance from the neuron, it is difficult to isolate the contributions of dendritic depolarization from the noise floor on recording sites distant from the soma/axon hillock. Here, we introduce a technique to identify dendritic contributions to the potential recorded on distant electrode sites, providing additional information about the morphology of a recorded neuron in space with respect to the electrode array.

---

* This article is in preparation. Authors: Nicholas B. Langhals, Kip A. Ludwig, and Daryl R. Kipke.

To evaluate this technique, we implanted silicon microelectrode arrays (NeuroNexus Technologies) in the motor cortex of Sprague Dawley rats and auditory cortex of guinea pigs. The implanted microelectrode arrays had site locations enabling recording from multiple locations at multiple cortical depths simultaneously. To apply our technique, we first identified well-isolated unit activity on a specific site. Using the known firing times of the well-isolated unit, we were able to identify the contributions of the recorded neuron to the noise floor on distant recording sites. Electrode locations dorsal and ventral to the site with a well-isolated spike exhibited a contribution to recorded potentials, including the characteristic flipping of the recorded waveform at distant locations. Electrodes located at the same cortical depth as the isolated action potential from a vertically oriented neuron exhibited almost no contribution to recorded potentials. This finding is consistent with the theorized contributions to the recorded extracellular potential of axonal and dendritic projections, which can span multiple cortical layers.

These results indicate that the potential fall off of a neuronal action potential is not analogous to homogenous fall off from a point source, but is instead influenced by neuronal morphology. Moreover, we demonstrate that the contribution of neuronal morphology to the extracellular potential can be detected by recording at precise locations dorsal to the site putatively recording from the cell body. Consequently, the methodology introduced here may enable more precise spike sorting techniques.

I. INTRODUCTION

Detection of neural action potentials registered by a single recording electrode is typically accomplished through a threshold crossing process (Lewicki 1998) Ideally, a threshold line is set such that voltage perturbations generated by a neuron near a recording electrode during an action potential cross the threshold level, while background noise from other sources do not cross the threshold. As the largest focalized voltage perturbation generated by a neuron during an action potential occurs at the soma/axon hillock, standard thresholding techniques emphasize those contributions. While emphasizing the largest signal, the smaller amplitude contributions along the axons and dendritic arbors also nearby an electrode may be minimized or ignored entirely.

In many cases, it is desirable to also observe the voltage contribution of axons and dendritic arbors across multiple electrodes in order to: a) separate the action potential generated by a neuron from other action potentials with similar waveforms generated from other nearby neurons, b) identify the types of neurons being recorded from such as pyramidal cell or stellate cell and c) build a clearer picture of the in-vivo morphology of a neuron relative to multiple recording electrodes without performing histology. To accomplish this, twisted wires – two microwires to form a stereotrode or four wires to form a tetrode [Gray 1995, McNaughton 1983, Harris] – are extensively used in neuroscience research to create a cluster of multiple, closely-spaced sites (usually approximately 50 micron spacing) at the end of a single multi-strand wire.

When an action potential that crosses threshold is observed on one of the four wires, a “snapshot” on the other three wires is simultaneously recorded, allowing an experienced user to detect sub-threshold contributions of the neuronal action potential on the other electrode sites that are still large enough to differentiate from noise. Tetrode recording techniques have two obvious limitations, 1) the close spacing of the tetrodes make them ill-suited to detect the axonal and dendritic contributions of neurons such as pyramidal cells with processes that span multiple cortical layers or columns, and 2) when using an instantaneous “snapshot,” sub-threshold voltage contributions of neuronal processes on other sites can easily be obscured by sources of noise.

In this study, we introduce a technique known as “spike triggered averaging” (STA) that in combination with densely packed “Michigan” two-dimensional and three dimensional arrays addresses these known limitations to tetrode recordings. Using STA, we can easily isolate very small voltage contributions of a neuronal process nearby distant electrode sites by removing noise sources not strongly correlated to the firing of a specific neuron almost entirely. This, in conjunction with high-resolution 2-d and 3-d “Michigan” probes, allows us to develop a high resolution 2-d or 3-d morphological picture of the recorded neuron relative to the recording electrodes, capable of spanning multiple cortical layers and/or cortical columns in a chronically implanted setting. This additional information can then be used to differentiate neuronal cell types, determine neuronal stability over time, identify neuronal connectivity, address issues of plasticity, and address basic neuroscience questions involving in-vivo

chronic neuronal morphology in an intact system.

II. METHODS

A. *Microelectrodes*

All data used in this study was taken from either Sprague-Dawley rats or guinea pigs. The subjects were implanted with silicon 'Michigan' microelectrode arrays, using experimental procedures outlined previously (Vetter, Williams et al. 2004; Ludwig, Uram et al. 2006). Arrays consisted of one, four, or sixteen shanks, each with 4-16 evenly spaced iridium electrodes (Figure III-1). Site and shank separation distances were adequate to limit the probability of an individual neuron being directly recorded from multiple sites as they were spaced at least 100 microns from each other in all three dimensions (Henze, Borhegyi et al. 2000). Sites on four shank probes were spaced at 200 microns in both directions, while single shank device sites were spaced at 100 microns. The 3D arrays used in this study consisted of prototype 3D probes assembled by NeuroNexus Technologies (Ann Arbor, MI). These were created by horizontally stacking four commercially available acute devices using a polymer interconnect to separate the individual probes for uniform spacing. Sixteen electrode shanks of four sites each were arranged in a 4x4x4 grid for a total of 64 electrode sites. The individual shanks were three millimeters in length with 177 μm^2 sites spaced at 100 µm apart along a shank, with shank spacing of 125 and 300 in each direction (Figure III-1).

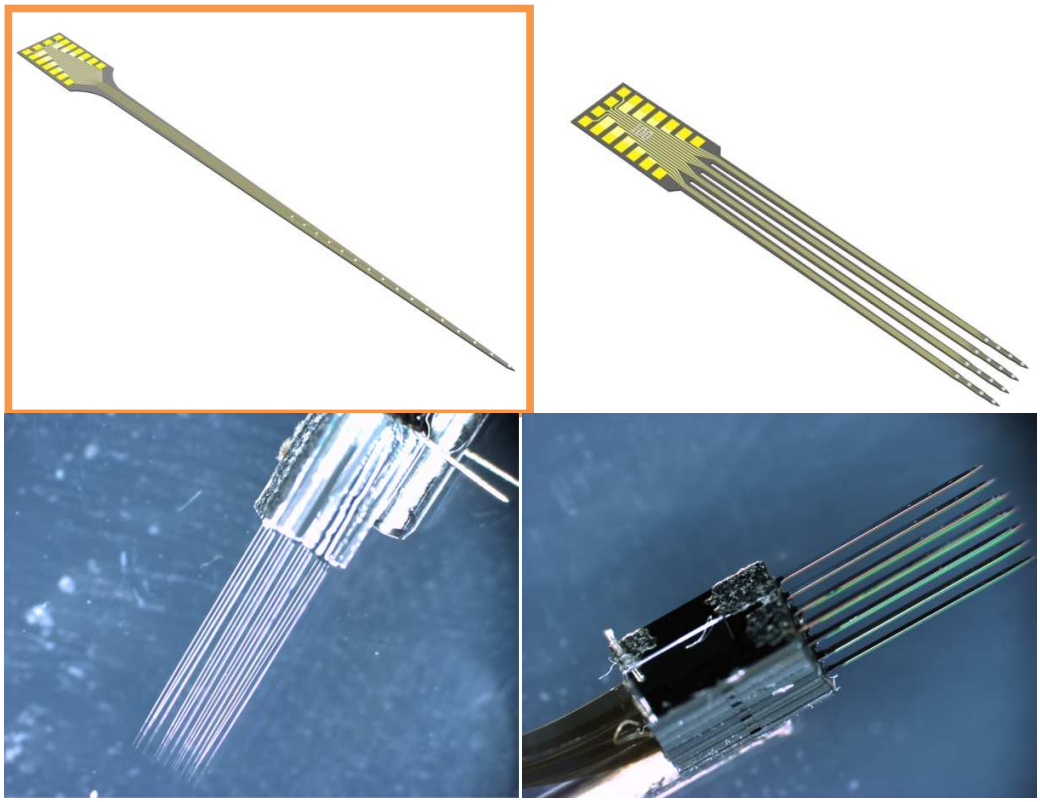

Figure III-1: Examples of site layouts of silicon probes used in this study. All device were provided by NeuroNexus Technologies, Inc., (Ann Arbor, MI). Image of example 3D probe style as used in this study consists of 4 rows of 4 shanks spaced at 125 µm between shanks and each row of shanks spaced at 300 µm.

B. *Surgical Techniques*

All implants in this study were performed on 250 - 300g female guinea pigs targeting primary auditory cortex. Surgical procedures were similar to those used previously (Vetter, Williams et al. 2004; Ludwig, Miriani et al. 2009; Kim, Wiler et al. 2010). Initial anesthesia was administered via intraperitoneal injection of a mixture of 40 mg/kg ketamine and 5 mg/kg xylazine. Updates were given throughout the procedure every hour or as needed to maintain a consistent depth of anesthesia. To prepare the implant location, the surface of the head was first shaved and the skin and connective tissue on the surface of

the skull were cleared. Next, three stainless steel bonescrews were secured in the skull anterior to bregma, and a bolt was then affixed to these screws using dental acrylic for the purpose of securing the head to a manipulator.

After securing the animal, a craniotomy approximately 4 x 4 mm was made over primary auditory cortex. The dura was resected in order to allow for probe insertion and the exact target was located using the well-defined vascular landmarks that have been reported previously. The 3D electrode array was then mounted to the stereotaxic manipulator and driven perpendicular to the cortical surface in to a target depth of about 1 mm so that the deepest electrode sites were located near layer IV. Last, a stainless steel needle was inserted into the skin tissue of the upper back and used as a reference and ground for all recordings in the experiment. All procedures complied with the U.S. Department of Agriculture guidelines for the care and use of laboratory animals and were approved by the University of Michigan Animal Care and Use Committee.

C. *Electrophysiology*

All recordings were acquired using a TDT multi-channel acquisition system (RX5, Tucker-Davis Technologies, Alachua, FL) in an electrically and acoustically shielded booth. Neural electrophysiological recordings for all 64 channels were fed through an anti-aliasing filter (0.35 Hz – 7.5 kHz) amplified, and sampled at ~25 kHz. Wideband data for post-processing unit characterization was left unfiltered.

D. *Data Filtering and Analysis*

Wideband neural recording segments were analyzed off-line using custom automated MATLAB (Mathworks, Natick, MA) software, as described in detail elsewhere (Ludwig, Miriani et al. 2009; Rohatgi, Langhals et al. 2009). Briefly, an amplitude discrimination threshold was set at 3.5 standard deviations above and below the mean of the recording segments. For each peak exceeding the threshold, a 2.4-ms candidate waveform snippet centered on the absolute minimum of the waveform was removed from the recorded segment and stored. The peak-to-peak noise level was calculated as six times the standard deviation of the remaining data. After initial principal component analysis, individual clusters were identified using fuzzy c-means clustering. After clustering, waveforms with a cluster membership index of greater than 0.8 were used to determine a mean waveform for a cluster. The signal-to-noise ratio for these waveforms was calculated as the peak-to-peak amplitude of the mean waveform divided by the calculated noise value. Values of greater than 1.1 were considered quality units, easily discriminable from the underlying noise floor.

E. *Impedance Spectroscopy Measurements*

Impedance spectroscopy measurements were made using an Autolab potentiostat PGSTAT12 (Eco Chemie, Utrecht, The Netherlands) with associated frequency response analyzer (Metrohm USA, Inc). Impedance measurements were made by applying a 25 mV RMS sine wave with 1-kHz

frequency. Prior to implantation, measurements were made by immersing the electrode recording sites in 0.1 M phosphate buffer saline (PBS) and a platinum foil was used as the reference electrode.

F. *Spike Triggered Averaging*

The basic concept behind using a spike triggered average (STA) has been used previously in other studies examining the relationships of local field potentials (LFPs) to activity from individual neurons (Donoghue, Sanes et al. 1998; Gail, Brinksmeyer et al. 2004; Magill, Sharott et al. 2004; Nelson, Pouget et al. 2008). The basic premise behind these and similar studies is to examine the changes in low frequency cortical activity as they relate to individual neural action potentials (spikes) recorded and sorted from the same electrode site, though at a substantially lower frequency. While information in local field potentials can be difficult to decipher with a single repetition, repeated examination of correlations between spikes and LFPs through averaging results in a net averaging effect removing the uncorrelated signal and noise within the LFP, while leaving the desired information about related information between the two distinct neural signals.

To apply our novel application of this technique, we first identified well-isolated unit activity on all sites on the electrode array, one at a time (See Methods). As the largest voltage perturbation generated by a neuron during an action potential occurs at the soma/axon hillock, one can assume the electrode on which the well-isolated unit is observed is near the soma/axon hillock. Next, a 5

ms window (or “snapshot”) of the voltage traces for all other channels on the array was obtained and stored, centered on each firing time from a well isolated unit. For example, if a well isolated unit was recorded at time t=100ms into the recording session on channel 1, a window from 97.5-102.5 ms (100ms +/- 2.5 ms) was stored from channels 2-16 (or 64). Finally, all of the “snapshots” for a given channel were averaged to generate the mean voltage trace over time on that channel resulting from the firings of the well-isolated action potential. By averaging over many firings, consistent low amplitude voltage perturbations resulting from dendritic contributions of the source neuron on nearby and distant channels remain, whereas random noise sources on these channels uncorrelated to the firing of the neuron average to nearly zero. After all steps, this process was then repeated for every well-isolated unit recorded on the array.

III. RESULTS/DISCUSSION

A. *STA from 2D Arrays*

In this study we utilized spike triggered averaging (STA) across multiple different electrode platforms to elucidate underlying neuronal morphology. Using STA, low amplitude voltage contributions of axons and dendrites to electrode sites distant from the soma/axon hillock, that were previously obscured by noise, become visible. Through STA, neural features that are correlated to the source channel remain, while all uncorrelated signal and noise diminishes to nearly zero. This method enables projections from the neuron to

be detected, yielding information about neural cell type and morphology.

The first dataset processed using STA was from two-dimensional planar arrays as shown in Figure III-1. Two different phenomena were observed using these arrays. First, a recorded action potential from a neuron with a horizontal projection was detected (Figure III-2 A). This signal from the projection of the neuron remains visible only at Depth 2 of the planar array and decreases in intensity further away from the assumed contribution of the soma. Note that the average voltage contribution from the horizontal projection is lower amplitude than the green noise level. Without application of our STA technique, this potential would not have been detectable. Given the structure of this field we are not able to determine the type of cell that is generating this potential field, but we do have a better understanding of the cell structure in the environment surrounding the electrode array.

In Figure III-2 (B) a different neuronal morphology across the array is evident, consistent with a pyramidal cell. Schmidt and Humphrey reported action potential shapes that would be theoretically recorded from pyramidal and stellate cells as an individual electrode was moved past the cell within the brain(Schmidt and Humphrey 1990). The example potential field that was reported for a pyramidal cell closely matches our STA plot below (Figure III-2). The red source channel has a waveform shape typically produced from the soma of a neuron. This signal then decreases to zero as the field is sampled near to the axon hillock, at which point the waveform shape inverts – known as

flipping - and the field becomes detectable again on the lower channel on the array. Note on the lowest site of the third shank this neuron's contribution to the potential field is actually higher amplitude than the noise floor on that channel, indicated in green. Using typical sorting and data analysis techniques, this action potential would be detected and likely classified as an independent, well-isolated single unit. However, the voltage deflection on this channel is actually generated by the same neuron seen from the second site on that shank. Counting the contribution of one neuron on an array twice would have the net result of artificially inflating the yield of the implanted device, as the second observation of the same unit is only capable of providing redundant information.

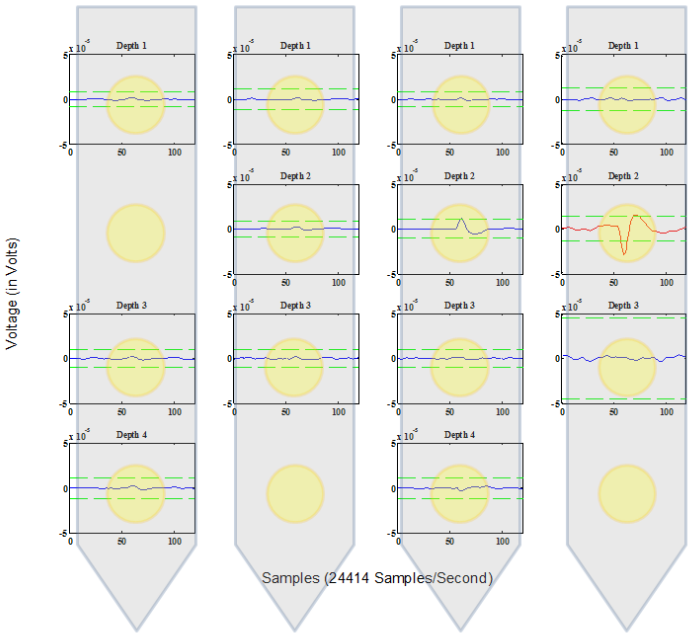

(A)

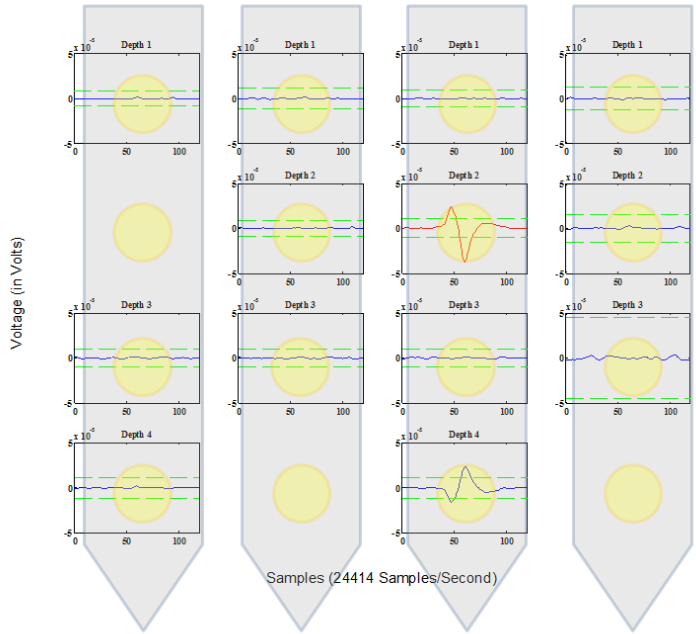

(B)

Figure III-2: Two plots of STA of four shank arrays. Red units indicate source of the STA, blue traces are averages on other channels, and green dashed lines indicate noise levels on the electrode sites. (A) Upper plot displays a horizontal projection from the source channel. (B) The lower plot has a flipping and signal propagation structure consistent with a pyramidal cell type.

Spike triggered averaging analysis was also applied to electrode arrays with 16 linearly spaced sites in a single cortical column (Figure III-3). In the left plot, the characteristic flipping occurs between the fourth and fifth site from the bottom. This indicates that the red source channel is likely recording from a pyramidal cell as well, though in this case the neuron is further from the electrode array than it was in the lower plot of Figure III-2, resulting in decreased amplitude at the soma and smaller contributions from distant neuronal processes. The right plot displays a similar effect, though the original waveform shape has a less pronounced positive deflection. However, the characteristic flipping in the STA shape on the blue channels is still visible. Inversion of the voltage waveform indicates that the signal is not simply the detection of the soma from further away, but is instead the observation of the potential field generated by neuronal processes other than the soma.

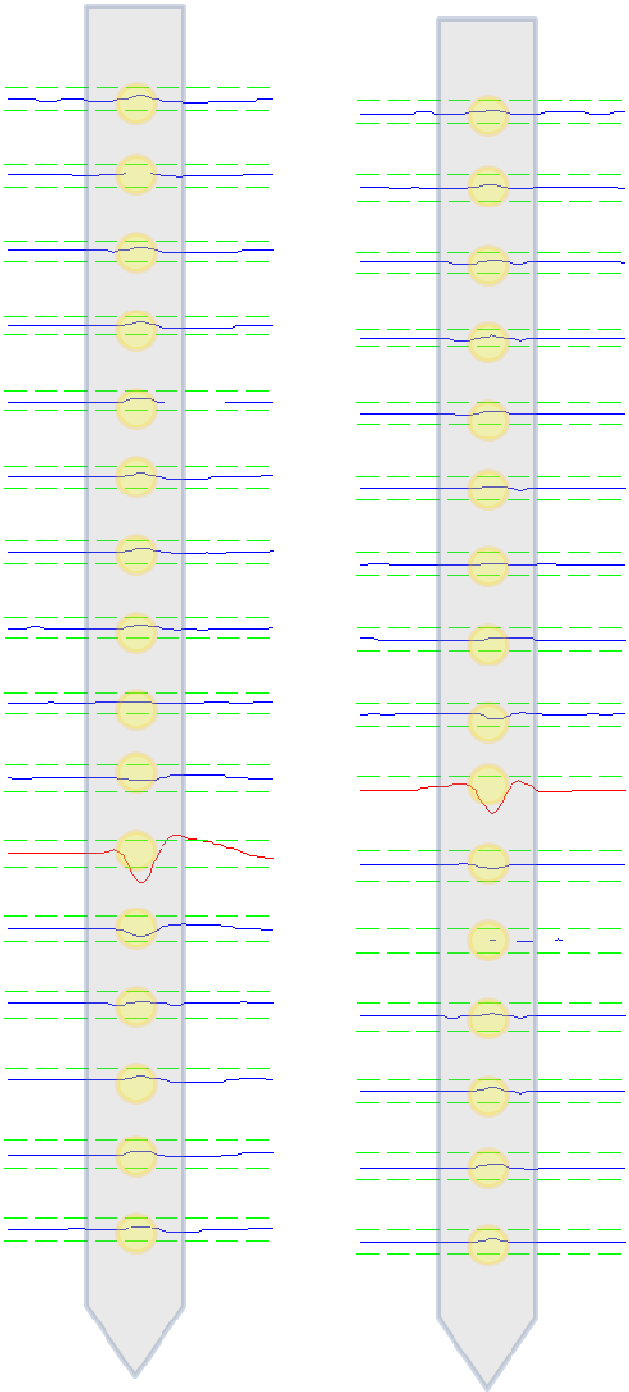

Figure III-3: Two separate STA plots created from single shank arrays. Red units indicate source of the STA, blue traces are averages on other channels, and green dashed lines indicate noise levels on the electrode sites.

B. *3D Probe Impedance*

For all 3D probes used in this study, electrode impedance was measured to verify that sites showing similar activity were not simply the result of shorting between electrodes on the array or within the connector assembly. Channels 40, 55, and 60 had impedances significantly higher than the average of the remainder of the sites and were excluded from further analysis. Channels 45 and 47 had extremely low impedances, likely the result of shorted sites and were also excluded.

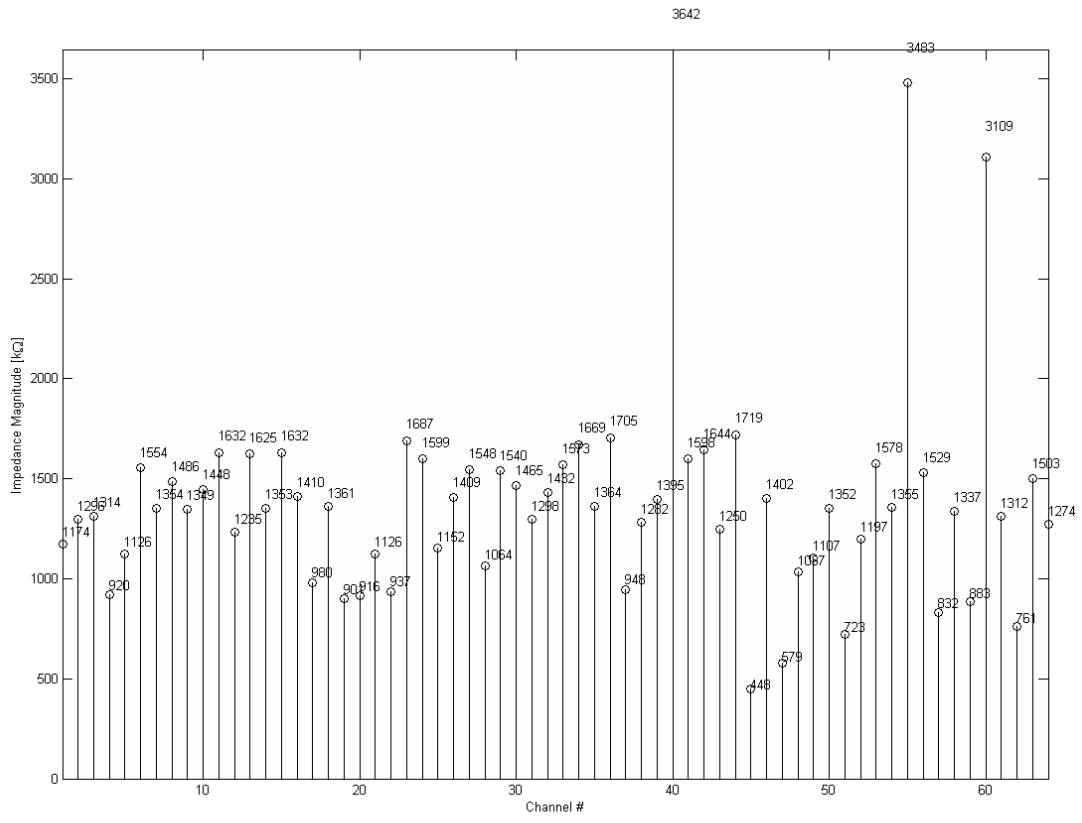

Figure III-4: 1 kHz Impedance magnitude of all 64 channels of electrodes sites used for the 3D data in this study.

C. *3D STA*

Using the sixteen shank 3D probes as outlined in the methods, we were able to replicate the 2D experimental data shown above (Figure III-2). Our 3D probes electrode sites were spaced at a smaller distance within a plane, 100 microns along the shank and 125 microns between shanks. Using this smaller spacing, we were able to detect a large pyramidal cell with an SNR of 1.7 as shown in the red starred plot of Figure III-5. The characteristic flipping indicative of neural morphology of a pyramidal cell (Schmidt and Humphrey 1990) is visible from the blue starred plot. In contrast to Figure III-2 (B), there are two sites between the evident flipping of the STA instead of one since the site spacing of the 3D probe is 100 microns as opposed to the 200 microns used for the 2D arrays. This result indicates that this neuron is likely of the same type and a similar distance in space from the implanted array. Horizontal and vertical propagation of the fields generated by the pyramidal cell are visible in plots labeled yellow.

Due to the organizational structure of the brain, we initially speculated that STA waveforms would be present on multiple planes within the array. From the lower plot of Figure III-5, we were unable to observe this effect. Based on modeling experiments currently underway within our research group (manuscript in preparation), we have determined that the organization of the electrode sites on the surface of each planar array results in an effective attenuation for signals present behind the planar array. While a single shank or

plane of the array can run parallel to projections from a neuron, it is unlikely for a neuronal process to run directly by two electrodes on separate planes after implantation. Assuming this effect also applies to the 3D arrays used in this study, it is unlikely that we can detect these extremely small signals, even if present, due limitations of neural recording hardware. Next generation 3D probe designs that incorporate planes of electrode sites that face each other would mitigate this problem and could allow us to examine fully three-dimensional structure of neurons present in the environment surrounding the implanted probe without the use of fMRI, tissue slice microscopy, or other high resolution imaging techniques.

Planned future applications for STA will explore synaptic connections between neurons by increasing the window size for the STA beyond the currently used 5 milliseconds. Theoretically, it may be possible to map out multiple connected neurons within the 3D space surrounding the electrode array using STA that were previously obscured by noise. This electrophysiological data could then be used to create a map of neural structure surrounding the implanted probe. There are however limitations to this technique that must first be addressed. First, the process is highly dependent on consistent spike firing times, even within the same cell. For example, while the mean time from the beginning of the dendritic potential to the initiation of a full action potential at the axon hillock may be 1 millisecond, any variation in this timing means that the voltage contribution of the dendrites can be inconsistently located in time, and therefore can be attenuated by the averaging process. Even with small amounts of

variability in propagation time, the observed STA waveform may change resulting in an inability to correctly identify cellular type.

With high resolution recording systems currently available, even extremely small contributions should be detectable using STA, but there is an inherent minimum detectable level using this technique. As the spike waveforms become smaller or are at a further distance from the array, the potential falloff from the dipole field generated by the neuron becomes the limiting factor. While the limit of detection of any neural signal is definitely greater than the 50 microns reported by (Henze, Borhegyi et al. 2000), the true limit still needs to be clarified. Even in a zero noise environment, ionic currents have a limited range of propagation, so that if no signal is reaching the electrode site, there is no averaging technique that would allow us to map the neural source.

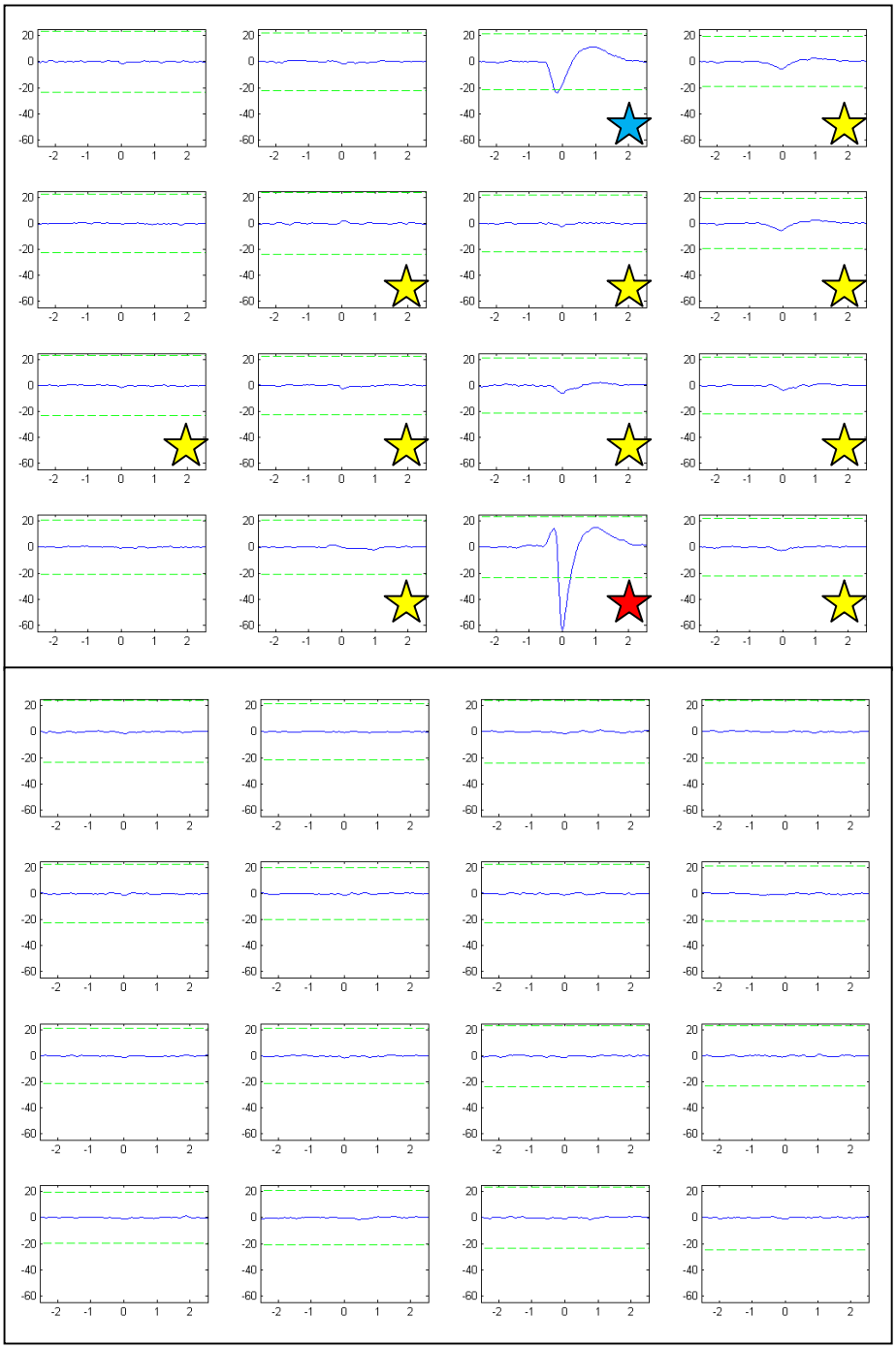

Figure III-5: STA plots from 3D probe implanted in guinea pig primary auditory cortex. The upper plot is from the front-most plane of the array with the red star indicating the source channel for the STA. The characteristic flipping is evident, particularly on the blue starred channel, with the yellow starred plots showing small contributions and propagations. On the lower plot, which is 300 microns back from the upper plot, no signal is visible.

IV. CONCLUSIONS

Within this study, we have taken advantage of the consistent dimensions of microfabricated arrays to explore the morphology of neurons through electrophysiological analysis. The ability of the 'Michigan' probe to record from multiple cortical depths simultaneously enables sampling from an individual neuron at multiple points. Through this simultaneous sampling, the contribution of the neuronal potential at an electrode can be visualized within the noise using spike triggered averaging of the wideband neural signal over multiple spike repetitions. The STA waveform that results from this process depends heavily upon neuronal morphology with respect to the electrode; therefore, cell types may be identified and the neuronal processes can be localized in two dimensional space. Through the application of STA, we have verified that neurons do not behave as point sources. Instead, the fields generated at different locations along the cell have different shapes that can be detected at distances of greater than 1 millimeter from the soma. This distance depends heavily on the orientation of the cell relative to the array, but can be much larger than the previously reported maximum detectable distance of 50 microns(Henze, Borhegyi et al. 2000).

The results of this study may heavily influence future neuroprosthesis designs. Through the use of this technique, we have a much greater understanding of how uniform site spacing and placement can be utilized to understand the

morphology of the brain providing new information compared to what is possible with current tetrode technologies. Furthermore, we have discovered that with sites spaced at distances around 100 microns that the same neuron may be detected on multiple electrodes. For neuroprosthetic systems focused on independent information channels, such as brain-machine interfaces, it has typically been assumed that these separations were sufficient to prevent the same neuron from being recorded from multiple sites simultaneously; however, this is not the case. For practical applications, either STA or cross correlations of firing times across all electrode sites must be employed to examine information content, or electrodes must be spaced even further away from each other to prevent simultaneous recordings of the same neural source. While small contributions may be detectable up to one millimeter away, these are insufficient to cross threshold with current noise levels. However, if biological and other noise sources decrease in future devices, extremely small potentials may once again become detectable. Subsequently, in neurophysiological applications using tetrodes, examining simultaneous activity on other tetrode arrays at distances of greater than 100 microns could yield more information about cell types; this information could then be used to create a full 3D reconstruction of cell type and location relative to the array to be compared and validated with immunohistochemistry.

V. ACKNOWLEDGEMENTS

The authors of this paper would like to acknowledge all of the members of the

Neural Engineering Laboratory at the University of Michigan for their assistance in this study.

VI. GRANTS

This work was supported by the NIH P41 Center for Neural Communication Technology (EB002030) and the Whitaker Foundation.

VII. DISCLOSURES

Daryl R. Kipke has significant financial interest in NeuroNexus Technologies, a leading supplier of microelectrode technology. Nicholas B. Langhals was a consultant for NeuroNexus Technologies. Sarah Richardson-Burns and Jeffrey Hendricks have significant financial interest in Biotectix, a company that specializes in conductive polymer coatings for electrodes.

VIII. REFERENCES

Donoghue, J. P., J. N. Sanes, et al. (1998). "Neural discharge and local field potential oscillations in primate motor cortex during voluntary movements." J Neurophysiol **79**(1): 159-173.

Gail, A., H. J. Brinksmeyer, et al. (2004). "Perception-related modulations of local field potential power and coherence in primary visual cortex of awake monkey during binocular rivalry." Cereb Cortex **14**(3): 300-313.

Henze, D. A., Z. Borhegyi, et al. (2000). "Intracellular features predicted by extracellular recordings in the hippocampus in vivo." J Neurophysiol **84**(1): 390-400.

Kim, D. H., J. A. Wiler, et al. (2010). "Conducting polymers on hydrogel-coated neural electrode provide sensitive neural recordings in auditory cortex." Acta Biomater **6**(1): 57-62.

Lewicki, M. S. (1998). "A review of methods for spike sorting: the detection and classification of neural action potentials." Network-Computation in Neural Systems **9**(4): R53-R78.

Ludwig, K. A., R. M. Miriani, et al. (2009). "Using a common average reference to improve cortical neuron recordings from microelectrode arrays." J Neurophysiol **101**(3): 1679-1689.

Ludwig, K. A., J. D. Uram, et al. (2006). "Chronic neural recordings using silicon microelectrode arrays electrochemically deposited with a poly(3,4-ethylenedioxythiophene) (PEDOT) film." Journal of Neural Engineering **3**: 59.

Magill, P. J., A. Sharott, et al. (2004). "Synchronous unit activity and local field potentials evoked in the subthalamic nucleus by cortical stimulation." J Neurophysiol **92**(2): 700-714.

Nelson, M. J., P. Pouget, et al. (2008). "Review of signal distortion through metal microelectrode recording circuits and filters." Journal of Neuroscience Methods **169**(1): 141-157.

Rohatgi, P., N. B. Langhals, et al. (2009). "In vivo performance of a microelectrode neural probe with integrated drug delivery." Neurosurg Focus **27**(1): E8.

Schmidt, E. and D. R. Humphrey (1990). Extracellular Single-unit Recording Methods. Neurophysiological techniques. Clifton, N.J., Humana Press. **2:** 1-64.

Vetter, R. J., J. C. Williams, et al. (2004). "Chronic neural recording using silicon-substrate microelectrode arrays implanted in cerebral cortex." IEEE Trans Biomed Eng **51**(6): 896-904.

Vetter, R. J., J. C. Williams, et al. (2004). "Spike recording performance of implanted chronic silicon-substrate microelectrode arrays in cerebral cortex." IEEE Transactions on Neural Systems and Rehabilitation Engineering **52**(1).

Chapter IV

PEDOT polymer coatings facilitate smaller neural recording electrodes[1]

I. Abstract

We investigated using poly(3,4-ethylenedioxythiophene) (PEDOT) to lower the impedance of small, gold recording electrodes with initial impedances outside of the effective recording range. Smaller electrode sites enable more densely packed arrays, increasing the number of input and output channels to and from the brain. Moreover, smaller electrode sizes promote smaller probe designs; decreasing the dimensions of the implanted probe has been demonstrated to decrease the inherent immune response, a known contributor to the failure of long-term implants. As expected, chronically implanted control electrodes were unable to record well-isolated unit activity, primarily as a result of a dramatically increased noise floor. Conversely, electrodes coated with PEDOT consistently

[1] This article is in press in the Journal of Neural Engineering. Authors: Kip A. Ludwig, Nicholas B. Langhals, Mike D. Joseph, Sarah M. Richardson-Burns, Jeffrey L. Hendricks and Daryl R. Kipke. While I am not first author on this paper, I contributed substantially to its written content and analyzed the majority of the data using algorithms developed in Chapter II.

recorded high-quality neural activity, and exhibited a much lower noise floor than controls. These results demonstrate that PEDOT coatings enable electrode designs 15 microns in diameter.

II. INTRODUCTION

The utility of implantable microelectrode arrays is currently limited by the size of the individual electrode sites for a number of reasons. First, smaller electrode sites facilitate the development of more densely packed microelectrode arrays. At present, researchers are limited to sampling from a few neurons out of the billions of neurons which execute function in the brain(Kipke, Shain et al. 2008). As a result, the study of how large networks of neurons interact to produce biologically relevant behaviors is severely hampered. Similarly, the efficacy of modern neuroprosthetic devices is greatly dependent upon the observable number of neural inputs/outputs. Second, smaller electrode sites promote the design of smaller arrays, which in turn cause less damage upon implantation. Recent studies indicate that probe dimensions smaller than 12 microns minimize the reactive cell responses that negatively impact long-term neural recordings(Bernatchez, Parks et al. 1996; Sanders, Stiles et al. 2000; Seymour and Kipke 2007).

Unfortunately, decreasing the size of an electrode site increases the impedance, which can degrade recordings. Impedance impacts recordings primarily through two mechanisms: noise and shunt loss(Najafi, Ji et al. 1990). Noise at the electrode/electrolyte interface can arise from random fluctuations of charged

carriers - either electrons in an electrical conductor (known as Johnson or thermal noise), or ions in an electrolytic medium(Robinson 1968; Schmidt and Humphrey 1990; Kovacs 1994; Shoham and Nagarajan 2003; Hassibi, Navid et al. 2004). These fluctuations can be caused by Brownian motion of electrons, drift and diffusion of charged ions due to concentration gradients, oxidation/reduction reactions occurring at the electrode/electrolyte interface, etc(Hassibi, Navid et al. 2004). As these random movements occur they create current perturbations, which increase the voltage noise in proportion to impedance(Hassibi, Navid et al. 2004). Noise resulting from the fluctuation of charged particles (which we will refer to as fluctuation noise hereafter) represents only one source of noise out of many possible sources: instrumentation noise, shot noise, flicker noise, biological noise, etc. Sources of noise sum in quadrature ($a^2 + b^2 = c^2$), meaning that the single largest source of noise tends to dominate the noise floor. Functionally, this means that the fluctuation noise for an electrode will only marginally contribute to the total noise floor until a nominal impedance magnitude is reached. Beyond this impedance magnitude, fluctuation noise will tend to dominate the observed noise floor.

Shunt loss is defined as the loss of signal from the electrode and measurement system to ground. This can be separated into three distinct circuit elements. First, there is a capacitive loss from the metal traces on the microelectrode to the surrounding Cerebral Spinal Fluid (CSF)(Robinson 1968). Second, a resistive element models the loss of signal from the inherent resistive nature of the metal wiring from the electrode to the measurement system(Robinson 1968).

Finally, there is a capacitor that models the capacitive signal loss in the measurement system(Robinson 1968). Like fluctuation noise, shunt loss increases in proportion to impedance(Robinson 1968). Typically, electrodes with impedances of 5 MΩ or greater have levels of fluctuation noise and shunt loss that make recording from individual neurons problematic(Robinson 1968; Najafi, Ji et al. 1990; Hetke, Lund et al. 1994).

Conductive polymer coatings have been hypothesized to be an enabling technology for smaller electrode designs(Ludwig, Uram et al. 2006; Richardson-Burns, Hendricks et al. 2007; Cogan 2008; Keefer, Botterman et al. 2008; Wilks, Richardson-Burns et al. 2009; Abidian, Corey et al. 2010). Conductive polymers increase the electrochemical surface area of an electrode (ESA) without changing its geometric surface area (GSA - e.g. diameter, circumference), lowering impedance(Cui and Martin 2003; Richardson-Burns, Hendricks et al. 2007; Abidian and Martin 2008; Abidian, Ludwig et al. 2009). In 2006, the Kipke lab demonstrated that surfactant-templated poly(3,4-ethylenedioxythiophene) (PEDOT) could be used to improve chronic neural recordings from standard-sized electrodes(Ludwig, Uram et al. 2006).

Building on this earlier work, in this study we demonstrate that PEDOT coatings effectively lower the impedance of small, gold recording electrodes (15 microns in diameter) with initial impedances outside of the effective range. Chronically implanted unmodified electrodes were unable to record well-isolated unit activity, primarily because of an increased noise floor arising from large site impedances.

Conversely, sites coated with PEDOT were able to consistently record high-quality neural activity, and exhibited a markedly lower noise floor than controls.

III. METHODS

A. Microelectrodes

Three male Sprague-Dawley rats were implanted with three 16-channel chronic silicon 'Michigan' microelectrode arrays, using experimental procedures outlined previously(Vetter, Williams et al. 2004; Ludwig, Uram et al. 2006). Arrays consisted of four shanks, each with four evenly spaced gold electrodes. Site and shank separations were sufficient (100 µm or greater) to limit the probability of an individual neuron being recorded from multiple sites(Henze, Borhegyi et al. 2000). All electrodes used in this study were 15 microns in diameter, or a GSA of 177 μm^2.

B. Electrochemical Deposition & Initial Evaluation

Electrochemical deposition of PEDOT in this study was accomplished using an electrochemical potentiostat/ galvanostat (Autolab PGSTAT12, Eco Chemie, Urtecht, The Netherlands) with associated General Purpose Electrochemical System (GPES) software. PEDOT doped with tetraethylammonium perchlorate and dissolved in 20 wt% surfactant poly(oxythylene)10-oleyl ether was galvanostatically deposited onto the gold sites of the neural probes(Yang, Kim et al. 2005). Based on results from our prior paper, PEDOT films generated with a deposition charge of 260 mC/cm^2 were chosen for *in vivo* testing.

Scanning electron microscopy (SEM) demonstrated that the PEDOT film deposited using a charge of 260 mC/cm^2 did not increase the diameter of the recording site (Figure IV.1). Consequently, at 260 mC/cm^2 the PEDOT film increased the electrochemical surface area of the electrode (ESA) without increasing the geometric surface area (GSA). Eight sites on each probe were deposited with surfactant-templated ordered PEDOT film. The deposited sites were staggered in relative location to prevent bias due to specific shank location or cortical depth (Figure IV.3). The remaining eight sites on each probe were left uncoated as controls for comparison.

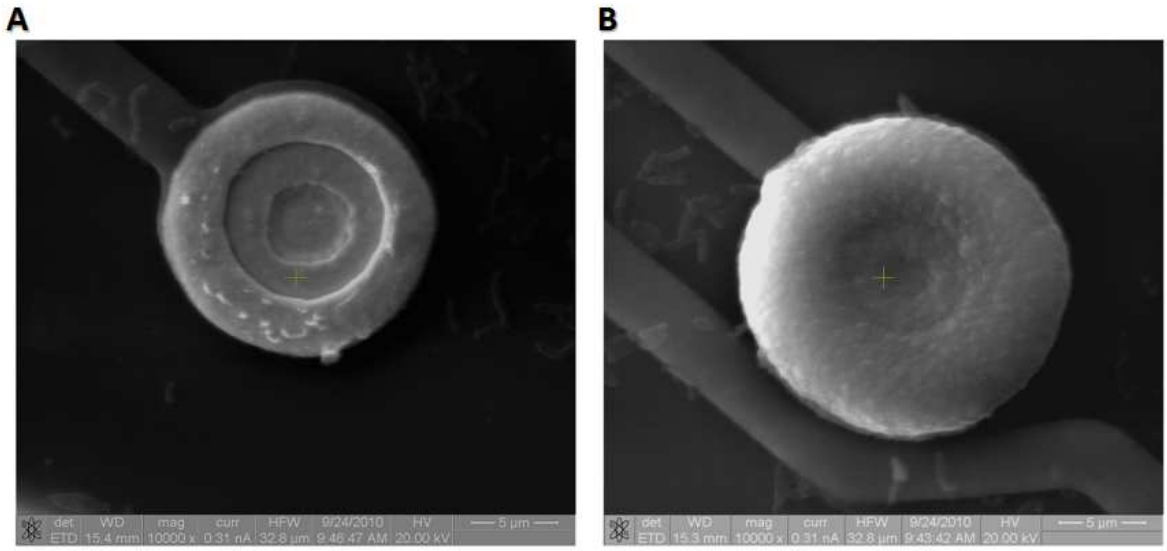

Figure IV-1: Scanning Electron Microscopy, PEDOT coatings. A) Depicts a PEDOT film generated using a deposition charge of approximately 260 mC/cm^2, and B) depicts a PEDOT film generated using a deposition charge of approximately 1600 mC/cm^2. Note that the PEDOT film generated using 260 mC/cm^2 does not increase the geometric diameter of the underlying gold site, whereas the film generated using a deposition charge of 1600 mC/cm^2 increases the effective diameter of the gold site by approximately 20 percent. For this study, PEDOT films were generated using a deposition charge of 260 mC/cm^2.

C. Surgical Techniques

All of the arrays in this study were implanted in motor cortex, targeting cortical layer V, as outlined in previous work(Vetter, Williams et al. 2004; Ludwig, Uram et al. 2006; Ludwig, Miriani et al. 2009) . Initial anesthesia was administered via intra-peritoneal injections of a mixture of 50 mg/ml ketamine, 5 mg/ml xylazine, and 1 mg/ml acepromazine at an injection volume of 0.125 ml/100g body weight. Updates of 0.1 ml ketamine (50 mg/ml) were delivered as needed to maintain anesthesia during the surgery. Animals were secured to a standard stereotaxic frame, and three stainless steel bone-screws were inserted into the skull. The electrode connector was grounded to a bone-screw over parietal cortex using a stainless steel wire.

A craniotomy approximately 3 mm by 2 mm was made over the target area (target location 3.0 mm anterior to bregma, 2.5 mm lateral from bregma, and 1.4 mm deep from the surface of the brain). Two incisions were made in the dura mater to create four flaps, which were subsequently folded back over the edge of the craniotomy. The electrodes were then hand inserted using microforceps into the approximate target cortical area. Cortical depth was estimated using the known location of the electrode sites on the individual shanks in conjunction with the known length of the individual shanks. Next, the surface of the brain was covered with GelFoam® (Henry Schein, Inc., Miami, FL) for protection. The silicon cable connector was covered with either remaining Gelfoam or Kwik-Sil silicone polymer (World Precision Instruments, Inc). The

entire assembly excluding the connector was then enclosed using dental acrylic (Co-Oral-Ite, Dental Mfg. Co., Santa Monica, Ca). Finally, sutures were used to close the skin around the acrylic and triple-antibiotic ointment was applied. All procedures complied with the United States Department of Agriculture guidelines for the care and use of laboratory animals and were approved by the University of Michigan Animal Care and Use Committee.

D. Neural Recordings & Data Analysis

Recorded neural signals were acquired using a Plexon Multi-channel Neural Acquisition Processor (MNAP; Plexon Inc, Dallas, TX). Neural electrophysiological recordings for all sixteen channels were amplified and bandpass filtered; single and multi-unit recordings were sampled at 40 kHz (Plexon), and bandpass filtered from 450-5000 Hz. All recordings were taken in reference to a distant stainless steel (316-SS grade) bone screw inserted through the skull during surgery. During recording sessions, animals were placed in an electrically shielded recording booth and multiple 30-second segments of continuous neural recordings were taken. Animals were lightly anesthetized with ketamine/xylazine throughout the data collection sessions.

Neural recording segments were analyzed offline to determine number of neurons recorded, noise levels, and signal amplitudes using custom automated MATLAB (Mathworks Inc., MA) software, as described in detail(Ludwig, Uram et al. 2006) and utilized elsewhere(Ludwig, Uram et al. 2006; Abidian, Ludwig et al. 2009; Langhals and Kipke 2009; Ludwig, Miriani et al. 2009; Purcell, Thompson

et al. 2009; Rohatgi, Langhals et al. 2009). In summary, an amplitude threshold window was set 3.5 standard deviations above and below the mean of the sample distribution. For each peak exceeding the threshold window, a 2.4 ms candidate waveform snippet centered on the absolute minimum of the waveform was removed from the recorded segment and stored. The amplitude of the noise voltage for every recording site in each recorded segment was calculated after all candidate waveforms had been removed.

After initial principal component analysis and fuzzy C-means clustering(Ludwig, Uram et al. 2006), waveforms with a cluster membership index of greater than 0.8 were used to determine a mean waveform for a cluster. An interspike interval histogram for each cluster was generated and visually inspected for an obvious absolute refractory period as an additional measure of noise rejection. Signal amplitude for a cluster was defined as the peak-to-peak amplitude of the mean waveform for each cluster.

The signal-to-noise ratio (SNR) for a given cluster was defined as follows:

SNR = Signal Amplitude / (2 * Calculated RMS Noise Voltage for Recording Site)

Clusters were then separated into one of four categories based on calculated SNR. Clusters with an SNR of greater than 4 were categorized as quality units. Clusters with an SNR between 3 and 4 were categorized as moderate units. Clusters with an SNR between 2 and 3 were categorized as poor units, while clusters with an SNR of less than 2 were not considered units. These four

categories correspond well with observations of unit quality based on signal-to-noise ratio made in similar recording studies (Henze, Borhegyi et al. 2000; Ludwig, Uram et al. 2006; Ludwig, Miriani et al. 2009).

Isolating action potentials from an individual neuron using an individual recording site is inherently prone to classification errors (Lewicki 1998; Harris, Henze et al. 2000). The methodology employed in this study is intended to minimize these errors, and should accurately parallel the true number of underlying neural sources. The sorting routine produces similar results to manual sorting performed by experienced researchers over the same data sets, but with the advantage of being objective and automated (Ludwig, Uram et al. 2006).

E. Impedance Spectroscopy Measurements

Impedance spectroscopy measurements were made using an Autolab potentiostat PGSTAT12 (Eco Chemie, Utrecht, The Netherlands) with associated frequency response analyzer (Metrohm USA, Inc). Impedance measurements were made by applying a 25 mV RMS sine wave with frequencies varied logarithmically from 10 Hz to 10 kHz. Prior to implantation, measurements were made by immersing the electrode recording sites in 0.1 M phosphate buffer saline (PBS) and a platinum foil was used as the reference electrode. After implantation, a distant stainless steel (316-SS grade) bone screw was used as the reference electrode.

F. Statistical Analysis

For this study, comparative statistical significance between groups was determined using standard analysis of variance techniques (ANOVA). There were 24 PEDOT modified sites and 24 control sites on any specific day in the experiment. The factors used in initial comparative ANOVA calculations for any given metric were: coated vs. control, animal, and day number. The associated calculated standard deviation has been included in the text with all average measurements.

IV.. RESULTS/DISCUSSION

G. Impedances

The impedances of the electrodes at 1 kHz were used for comparison purposes as action potentials have a characteristic frequency band centered at 1 kHz. Prior to implantation, the 1 kHz impedance of the unmodified gold sites ranged between 6-11 MΩ, with a mean impedance of 9.1±1.4 MΩ (See Table 1). After electrochemical deposition with PEDOT, *in vitro* site impedances ranged between 0.3 -0.6 MΩ, with a mean impedance of 0.37 MΩ±0.05.

Over the seven days following implantation, impedance increases were noted in both PEDOT and control sites that were consistent with trends observed in other microelectrode recording studies performed in the rat model(Vetter, Williams et al. 2004; Ludwig, Uram et al. 2006; Abidian, Ludwig et al. 2009; Ludwig, Miriani et al. 2009). Figure IV.2 depicts Bode plots of the average

impedance magnitude for PEDOT and control sites at Day 0, Day 4, and Day 7 post surgery. Over the first two days following implantation, the average impedance of the PEDOT sites at 1 kHz slightly increased to 0.45±0.1MΩ, while the average impedance of the control sites also slightly increased to 9.2±1.7 MΩ (p<0.001, See Table 1). Between days three and five post-implantation, a more marked impedance increase at 1kHz was observed on both PEDOT and control sites, to 1.31±0.4 MΩ and 10.3±1.9 MΩ respectively (p<0.001, See Table 1). During the peak of the early reactive response, spanning from days 6 to 8, the mean impedance of PEDOT sites further increased to 2.21±0.7 MΩ while the mean impedance of the unmodified sites also increased to 11.4±2.2 MΩ (p<0.001, See Table 1).

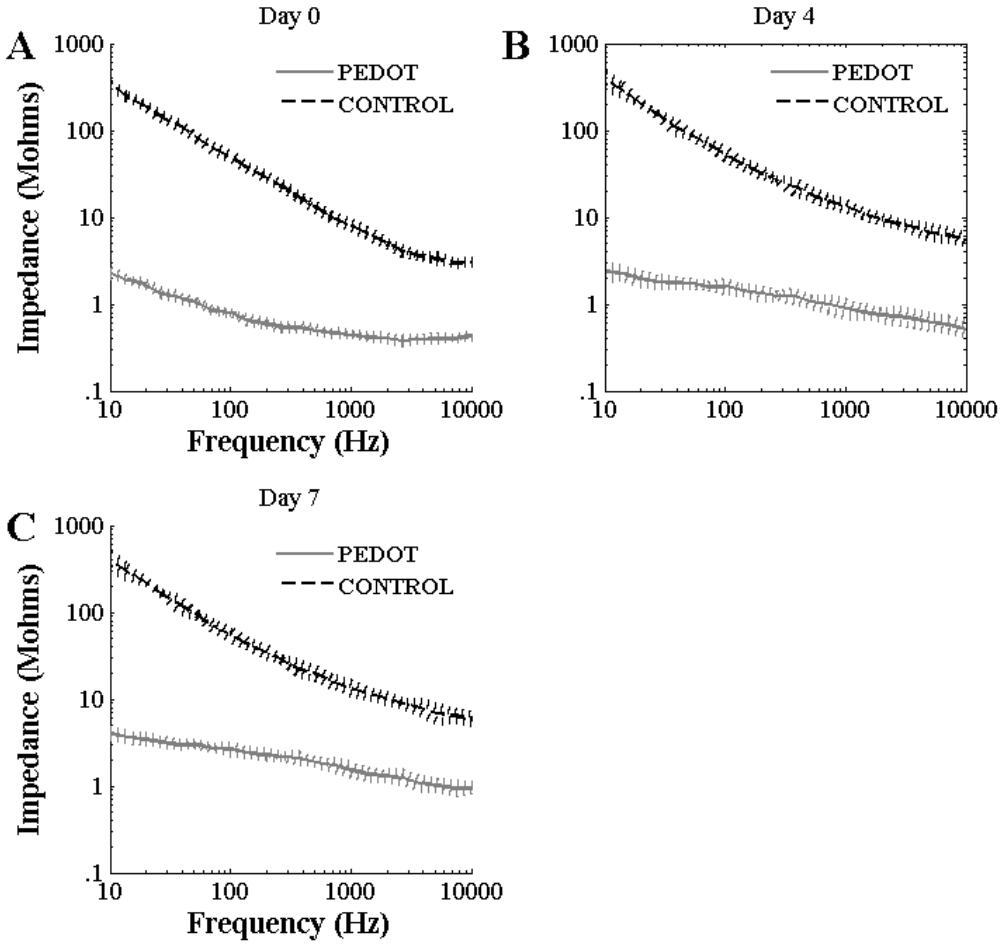

Figure IV-2. Bode plot of average measured impedance versus frequency. The dotted lines denote standard error of the data set on the given day (n=24). (a) Day 0 post-implantation. (b) Day 4 post-implantation. (c) Day 7 post-implantation. As the immune response to the implant progresses the first seven days from surgery, impedances at the critical 1 kHz frequency increase for both PEDOT and control sites.

H. Noise

As anticipated, the average peak-to-peak noise levels over the timeframe of this experiment were dramatically larger on control sites (Control Mean: 106.2±8.2 µV, PEDOT Mean: 35.3±5.3 µV). Over the seven days following implantation, the trend in average peak-to-peak noise levels on both PEDOT and control sites paralleled their impedance trends (See Table 1). In the period spanning days three and five post-surgery, the average peak-to-peak noise level on PEDOT sites increased to 46.2±8.1 µV, while control sites increased to 111.3±10.1 µV. During days six to eight post-surgery, the average peak-to-peak noise levels on PEDOT and control sites yet again increased, to 51.3±9.3 µV and 116.8±9.5 µV respectively.

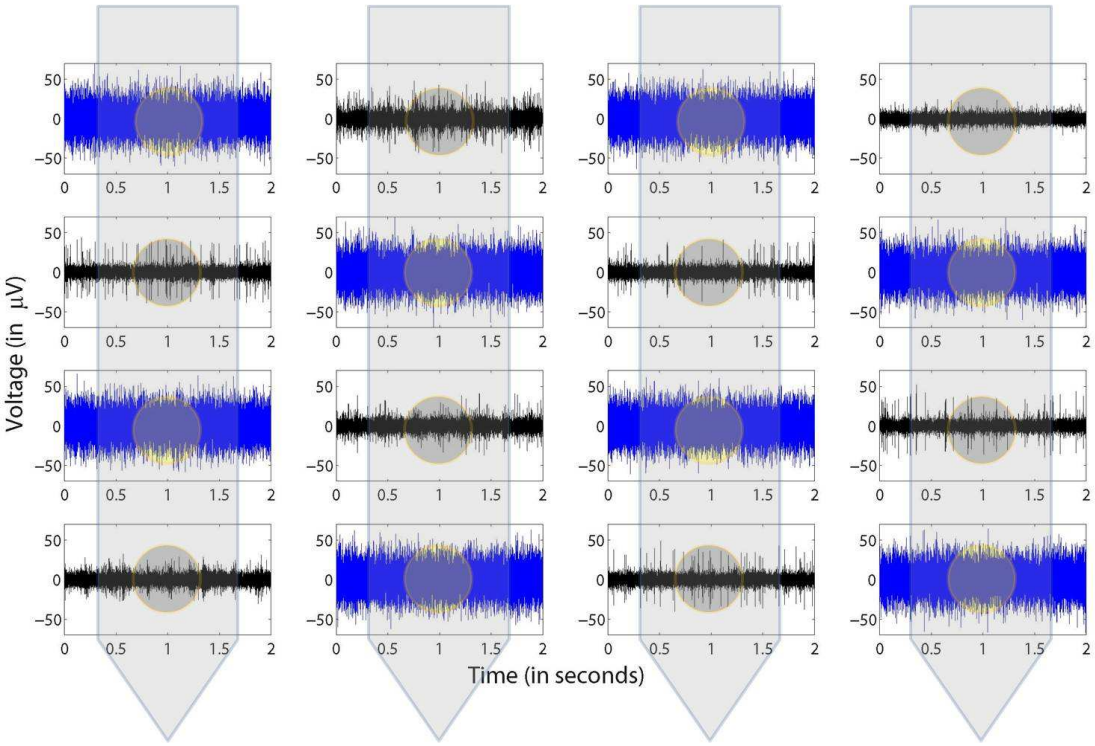

Figure IV-3: Representative High Speed Data Across One 4-shank Array. Black traces are PEDOT sites, while Blue traces denote Controls. The noise floor on control sites is dramatically larger than the noise floor on PEDOT sites, presumably obscuring unit activity.

I. Unit Recordings

Quality unit activity was evident on at least some PEDOT treated sites on all three arrays at every time point in this study (See Table 1). The average number of recorded units for PEDOT sites was highest in the days immediately following surgery (0.8±0.1 average units per site; total number of quality units/total number of sites), and then diminished over the week following surgery (0.4±0.2 average units per site between days 6 and 8 following surgery). A decreasing trend in unit activity in the week following surgery has been noted elsewhere (Ludwig, Uram et al. 2006; Santhanam, Linderman et al. 2007; Ludwig, Miriani et al. 2009; Purcell, Thompson et al. 2009) and is hypothesized to be caused by edema/swelling coupled with the initial immune response.

In contrast to the PEDOT sites on the three implanted arrays, no quality unit activity was evident on the control sites at any point during this study (see Table 1). Recordings on control sites were dominated by a large noise floor, which was sufficient to obscure all unit activity on these sites (see Figure IV.3). The high initial impedance of the untreated sites resulted in a large fluctuation noise contribution, dramatically reducing the likelihood of observing neural activity sufficient in amplitude to be differentiated from the noise floor.

Table IV-1: Summary of Results for Groups of Days after Surgery. PEDOT site averages are listed in *black*, while control site averages are listed in *blue*.

	Average Impedance (in MΩ)		Pk-Pk Noise (in µV)		Signal Amplitude (in µV)		Units per Site	
	PEDOT	Control	PEDOT	Control	PEDOT	Control	PEDOT	Control
Days 0-2	0.45±0.1	9.2±1.7	35.3±5.3	106.2±8.2	55.2±20.2	N.A.	0.8±0.1	0
Days 3-5	1.31±0.4	10.3±1.9	46.2±8.1	111.3±10.1	84±14.4	N.A.	0.5±0.2	0
Days 6-8	2.21±0.7	11.4±2.2	51.3±9.3	116.8±9.5	95.3±17.1	N.A.	0.4±0.2	0

J. Contribution of Encapsulation

Inserting a microelectrode into brain tissue elicits a reactive foreign body response, which produces a fibrous encapsulation of the array, effectively creating a high impedance barrier between the microelectrode and the neuron population (Liu, McCreery et al. 1999; Turner, Shain et al. 1999; Szarowski, Andersen et al. 2003). A well-described theoretical circuit model of this phenomenon has been widely accepted (Grill and Mortimer 1994; Buitenweg, Rutten et al. 1998; Otto, Johnson et al. 2006; Williams, Hippensteel et al. 2007). The tissue encapsulation of the array can be characterized by a sealing resistance, describing protein adsorption and in some cases a layer of connective tissue. In addition, the model incorporates adjacent cellular layers of glia and macrophages given by a membrane capacitance, a membrane resistance, and a membrane area scaling term, *m*, related to encapsulation

thickness and cell-to-cell adhesion within the cellular layer (See Figure IV.4). The extracellular pathway between cells is defined as a resistance.

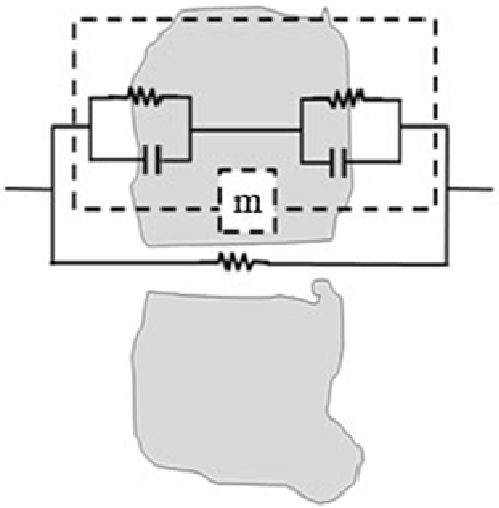

Figure IV-4: One Individual Element of the Lumped Circuit Model for Encapsulation.

Based on this model, the chronic foreign body response can dramatically increase the effective overall impedance of a chronically implanted electrode. In previous studies describing the changes in electrode impedance of typically-sized cortical microelectrodes following implant, the contribution of the encapsulation response to total electrode impedance became dominant after a few weeks (Vetter, Williams et al. 2004; Ludwig, Uram et al. 2006; Abidian, Ludwig et al. 2009; Purcell, Thompson et al. 2009). Consequently, increasing the pre-implant surface area using a conductive polymer coating provided limited chronic benefit to neural recordings (Ludwig, Uram et al. 2006).

In this study of small electrode sites 15 microns in diameter, the obvious benefit of PEDOT coatings to neural recordings was still evident at eight days post implant. This time point is important, as the contribution of encapsulation to electrode impedance typically reaches a maximum one to two weeks post surgery (Vetter, Williams et al. 2004; Ludwig, Uram et al. 2006; Abidian, Ludwig et al. 2009; Purcell, Thompson et al. 2009), demonstrating that PEDOT coatings enable neural recordings from small electrode sites even when the impedance contribution of encapsulation is at a maximum. These results indicate that as the size of the electrode decreases and total impedance approaches 5 MΩ and beyond, coatings to increase the surface area of the electrode become critical to minimize fluctuation noise and shunt loss.

Although the PEDOT films enabled recordings through 15 micron diameter sites, by day 8 the average number of quality units per PEDOT site had diminished to 0.4 units per site, presumably due to the inherent foreign body response to the electrode. Consequently, future work will focus on utilizing PEDOT coatings to enable smaller multi-electrode arrays that cause less damage upon implantation. Recent studies have indicated that by reducing the size of the implanted electrode, the foreign-body response to the electrode can be minimized, decreasing the contribution of encapsulation to impedance (Chen, Mrksich et al. 1997; Sanders, Stiles et al. 2000; Turner, Dowell et al. 2000; Seymour and Kipke 2007) and possibly limiting neuronal death in the vicinity of the electrode array (Biran, Martin et al. 2005). Although PEDOT is one enabling component of manufacturing smaller multi-electrode arrays, a number

of technical problems need to be addressed - e.g. insulation requirements, interconnect reliability, crosstalk between adjacent traces, etc. - before these arrays become a practical reality.

V. CONCLUSIONS

The next generation of neural electrodes needs to facilitate more channels of communication to and from the brain over a smaller tissue area. Moreover, these electrodes need to be smaller in order to limit neural damage upon implantation and long-term insult to the surrounding tissue. Current probe designs are limited to larger sizes to accommodate larger electrodes necessary to maintain lower electrode impedance and sustainable recordings. Furthermore, polymer device fabrication can be further optimized with fewer fabrication steps necessary by using a single gold metalization layer. However, recording from small gold electrode sites yields high noise levels and signal loss through shunt pathways, primarily due to the large associated impedances. In this study, PEDOT successfully decreased the impedance of previously unusable small gold electrode sites to within viable neural recordings range. PEDOT coatings help to alleviate this major electrode design constraint, enabling the fabrication of ultra-small, high-channel count, next-generation polymer arrays to interface chronically with the brain.

VI. ACKNOWLEDGEMENTS

The authors of this paper would like to acknowledge all of the members of the Neural Engineering Laboratory at the University of Michigan for their assistance in this study.

VII. GRANTS

This work was supported by the NIH P41 Center for Neural Communication Technology (EB002030) and the Whitaker Foundation.

VIII. DISCLOSURES

Daryl R. Kipke has significant financial interest in NeuroNexus Technologies, a leading supplier of microelectrode technology. Nicholas B. Langhals was a consultant for NeuroNexus Technologies. Sarah Richardson-Burns and Jeffrey Hendricks have significant financial interest in Biotectix, a company that specializes in conductive polymer coatings for electrodes.

IX. REFERENCES

Abidian, M. R., J. M. Corey, et al. (2010). "Conducting-polymer nanotubes improve electrical properties, mechanical adhesion, neural attachment, and neurite outgrowth of neural electrodes." Small **6**(3): 421-429.

Abidian, M. R., K. A. Ludwig, et al. (2009). "Interfacing Conducting Polymer Nanotubes with the Central Nervous System: Chronic Neural Recording using Poly(3,4-ethylenedioxythiophene) Nanotubes." Advanced Materials **21**(37): 8.

Abidian, M. R. and D. C. Martin (2008). "Experimental and theoretical characterization of implantable neural microelectrodes modified with conducting polymer nanotubes." Biomaterials **29**(9): 1273-1283.

Bernatchez, S. F., P. J. Parks, et al. (1996). "Interaction of macrophages with fibrous materials in vitro." Biomaterials **17**(21): 2077-2086.

Biran, R., D. C. Martin, et al. (2005). "Neuronal cell loss accompanies the brain tissue response to chronically implanted silicon microelectrode arrays." Exp Neurol **195**(1): 115-126.

Buitenweg, J. R., W. L. Rutten, et al. (1998). "Measurement of sealing resistance of cell-electrode interfaces in neuronal cultures using impedance spectroscopy." Medical & biological engineering & computing **36**(5): 630-637.

Chen, C. S., M. Mrksich, et al. (1997). "Geometric control of cell life and death." Science **276**(5317): 1425-1428.

Cogan, S. F. (2008). "Neural stimulation and recording electrodes." Annu Rev Biomed Eng **10**: 275-309.

Cui, X. and D. C. Martin (2003). "Electrochemical deposition and characterization of poly(3,4-ethylenedioxythiophene) on neural microelectrode arrays." Sensors and Actuators **B 89**: 92-102.

Grill, W. M. and J. T. Mortimer (1994). "Electrical properties of implant encapsulation tissue." Ann Biomed Eng **22**(1): 23-33.

Harris, K. D., D. A. Henze, et al. (2000). "Accuracy of tetrode spike separation as determined by simultaneous intracellular and extracellular measurements." J Neurophysiol **84**(1): 401-414.

Hassibi, A., R. Navid, et al. (2004). "Comprehensive study of noise processes in electrode electrolyte interfaces." Journal of Applied Physics **96**(2): 9.

Henze, D. A., Z. Borhegyi, et al. (2000). "Intracellular features predicted by extracellular recordings in the hippocampus in vivo." J Neurophysiol **84**(1): 390-400.

Hetke, J. F., J. L. Lund, et al. (1994). "Silicon ribbon cables for chronically implantable microelectrode arrays." Biomedical Engineering, IEEE Transactions on **41**(4): 314-321.

Keefer, E. W., B. R. Botterman, et al. (2008). "Carbon nanotube coating improves neuronal recordings." Nat Nanotechnol **3**(7): 434-439.

Kipke, D. R., W. Shain, et al. (2008). "Advanced neurotechnologies for chronic neural interfaces: new horizons and clinical opportunities." J Neurosci **28**(46): 11830-11838.

Kovacs, G. T. A. (1994). Introduction to the theory, design, and modeling of thin-film microelectrodes for neural interfaces. Enabling Technologies for Cultured Neural Networks. D. A. S. a. T. M. L. Academic)**:** 121–165.

Langhals, N. B. and D. R. Kipke (2009). "Validation of a novel three-dimensional electrode array within auditory cortex." Conf Proc IEEE Eng Med Biol Soc **2009**: 2066-2069.

Lewicki, M. S. (1998). "A review of methods for spike sorting: the detection and classification of neural action potentials." Network-Computation in Neural Systems **9**(4): R53-R78.

Liu, X., D. B. McCreery, et al. (1999). "Stability of the interface between neural tissue and chronically implanted intracortical microelectrodes." IEEE transactions on rehabilitation engineering **7**(3): 315-326.

Ludwig, K. A., R. M. Miriani, et al. (2009). "Using a common average reference to improve cortical neuron recordings from microelectrode arrays." J Neurophysiol **101**(3): 1679-1689.

Ludwig, K. A., J. D. Uram, et al. (2006). "Chronic neural recordings using silicon microelectrode arrays electrochemically deposited with a poly(3,4-ethylenedioxythiophene) (PEDOT) film." Journal of Neural Engineering **3**: 59.

Najafi, K., J. Ji, et al. (1990). "Scaling limitations of silicon multichannel recording probes." Biomedical Engineering, IEEE Transactions on **37**(1): 1-11.

Otto, K. J., M. D. Johnson, et al. (2006). "Voltage pulses change neural interface properties and improve unit recordings with chronically implanted microelectrodes." Biomedical Engineering, IEEE Transactions on **53**(2): 333-340.

Purcell, E. K., D. E. Thompson, et al. (2009). "Flavopiridol reduces the impedance of neural prostheses in vivo without affecting recording quality." J Neurosci Methods **183**(2): 149-157.

Richardson-Burns, S. M., J. L. Hendricks, et al. (2007). "Polymerization of the conducting polymer poly(3,4-ethylenedioxythiophene) (PEDOT) around living neural cells." Biomaterials **28**(8): 1539-1552.

Richardson-Burns, S. M., J. L. Hendricks, et al. (2007). "Electrochemical polymerization of conducting polymers in living neural tissue." J Neural Eng **4**(2): L6-L13.

Robinson, D. A. (1968). "The electrical properties of metal microelectrodes." Proceedings of the IEEE **56**(6): 1065.

Rohatgi, P., N. B. Langhals, et al. (2009). "In vivo performance of a microelectrode neural probe with integrated drug delivery." Neurosurg Focus **27**(1): E8.

Sanders, J. E., C. E. Stiles, et al. (2000). "Tissue response to single-polymer fibers of varying diameters: evaluation of fibrous encapsulation and macrophage density." J Biomed Mater Res **52**(1): 231-237.

Santhanam, G., M. D. Linderman, et al. (2007). "HermesB: a continuous neural recording system for freely behaving primates." IEEE Trans Biomed Eng **54**(11): 2037-2050.

Schmidt, E. and D. R. Humphrey (1990). Extracellular Single-unit Recording Methods. Neurophysiological techniques. Clifton, N.J., Humana Press. **2:** 1-64.

Seymour, J. P. and D. R. Kipke (2007). "Neural probe design for reduced tissue encapsulation in CNS." Biomaterials **28**(25): 3594-3607.

Shoham, S. and S. Nagarajan (2003). The Theory of Central Nervous System Recording. Neuroprosthetics: Theory and Practice. K. W. Horch and G. S. Dhillon. Singapore, World Scientific Publishing**:** 448-465.

Szarowski, D. H., M. D. Andersen, et al. (2003). "Brain responses to micro-machined silicon devices." Brain Research **983**(1-2): 23-35.

Turner, A. M., N. Dowell, et al. (2000). "Attachment of astroglial cells to microfabricated pillar arrays of different geometries." J Biomed Mater Res **51**(3): 430-441.

Turner, J. N., W. Shain, et al. (1999). "Cerebral astrocyte response to micromachined silicon implants." Exp Neurol **156**(1): 33-49.

Vetter, R. J., J. C. Williams, et al. (2004). "Chronic neural recording using silicon-substrate microelectrode arrays implanted in cerebral cortex." IEEE transactions on bio-medical engineering **51**(6): 896-904.

Vetter, R. J., J. C. Williams, et al. (2004). "Spike recording performance of implanted chronic silicon-substrate microelectrode arrays in cerebral

cortex." IEEE Transactions on Neural Systems and Rehabilitation Engineering **52**(1).

Wilks, S. J., S. M. Richardson-Burns, et al. (2009). "Poly(3,4-ethylenedioxythiophene) as a Micro-Neural Interface Material for Electrostimulation." Front Neuroengineering **2**: 7.

Williams, J. C., J. A. Hippensteel, et al. (2007). "Complex impedance spectroscopy for monitoring tissue responses to inserted neural implants." J Neural Eng **4**(4): 410-423.

Yang, J., D. H. Kim, et al. (2005). "Ordered surfactant-templated poly(3,4-ethylenedioxythiophene) (PEDOT) conducting polymer on microfabricated neural probes." Acta Biomaterialia **1**(1): 125-136.

Chapter V

Validation of a Novel Three-Dimensional Electrode Array within Auditory Cortex*

Two-dimensional electrode arrays have been used in a variety of basic research studies characterizing and examining the neurophysiology of the brain. Single channel and 2D probes have been used to successfully map the sensory and motor organization of many different regions of the brain. However, thorough mapping involves multiple electrode penetrations and multiple experimental sessions to accumulate enough data to understand the underlying function. Furthermore, mapping of connectivity across brain regions and within layers simultaneously is only possible through the use of multiple devices, and therefore could be more easily performed through the use of high-channel count 3D electrode arrays. These higher channel counts are also beneficial in brain-machine interface applications as they increase the number of information channels available given a single surgical implantation, while minimizing risk to

* This article is in preparation. Authors: Nicholas B. Langhals, James Wiler, Kip A. Ludwig, and Daryl R. Kipke.

the patient. Here we present a proof of concept validation of a 3D probe technology consisting of 16 silicon shanks in a 4x4 grid arrangement with four electrode sites per shank. This 3D array has been implanted in guinea pig primary auditory cortex and electrophysiological data are presented showing the utility of electrode sites spanning multi-lateral cortical space as well as cortical depth. Using these devices, we were able to successfully map the tonotopic space with fewer insertions than would have been necessary with single wires or 2D probe architectures.

I. INTRODUCTION

Neural probe technology enables many different clinical and research applications, from disease characterization to studies of underlying neurophysiology. The structural characteristics of the brain, as studied anatomically or through imaging, yield valuable information about the expected function of the underlying neural system (Kotter and Wanke 2005). However, imaging and anatomical characterizations lack the resolution and desired output metrics that are desirable to understand how the firing of individual neurons and ensembles combine to create sensory perception or even consciousness. Through the use of three-dimensional (3D) electrode arrays, it is hoped that more information can be extracted from neural recordings about connectivity, plasticity, and the underlying neural networks.

To better understand and interpret the neural firing patterns within the brain, new technological advances are required that incorporate the use of high

channel counts that can simultaneously sample from large populations of neurons to yield more information about the underlying cortical morphology and structure. Many neural probe technologies exist that incorporate high numbers of electrode sites assembled from a large number of individual microwires (Ulbert, Halgren et al. 2001; Schwartz 2004). While these technologies achieve the throughput of information necessary for controlling external devices and brain-computer interfaces, they lack the ability to sample from a three-dimensional volume of neural tissue simultaneously (Lebedev and Nicolelis 2006). Other microfabricated structures can sample high channel counts and have been used in cortical mapping experiments (Figure V-1 Top), but these devices are only capable of sampling from a planar representation of the cortex (Csicsvari, Henze et al. 2003; Blanche, Spacek et al. 2005; Aarts, Neves et al. 2008; Du, Riedel-Kruse et al. 2009; Ludwig, Miriani et al. 2009). Through experiments utilizing these planar devices, we have developed a greater understanding of the neurophysiology. However, the brain is obviously a three dimensional structure composed of connections and projections over several millimeters. The simultaneous sampling of neural tissue in 3D enables more thorough mapping of neural connections within the brain which in turn facilitates understanding of how these networks can create sensory perceptions from the firing of individual neurons.

In order to move towards 3D electrode sampling, we have tested a new 64-channel electrode array implanted into the auditory cortex of a guinea pig. The electrode array was validated in three different capacities within this study to

verify device utility and functionality following insertion. First, gross recording quality was examined immediately following insertion to verify that the trauma during insertion does not preclude recording neural activity, and therefore is consistent with similar probe technologies. Second, auditory-driven activity was used to verify that the device was implanted into an auditory cortical region of the brain and localized neural circuits remained intact. Finally, frequency response maps of the primary auditory cortex were constructed to verify a typical and unaltered tonotopic architecture. Tonotopic maps demonstrated consistent structure within each plane due to the small site and shank spacing, however substantial differences between planes were observed where spacing was greater.

II. Methods

A. *Electrode Array*

The electrode arrays used in this study consisted of prototype 3D probes assembled by NeuroNexus Technologies (Ann Arbor, MI). These were created by horizontally stacking four commercially available acute devices using a polymer interconnect to separate the individual probes for uniform spacing. Sixteen electrode shanks of four sites each were arranged in a 4x4x4 grid for a total of 64 electrode sites. The individual shanks were three millimeters in length with 177 μm^2 sites spaced at 100 µm apart along a shank, with shank spacing of 125 and 300 in each direction (Figure V-1).

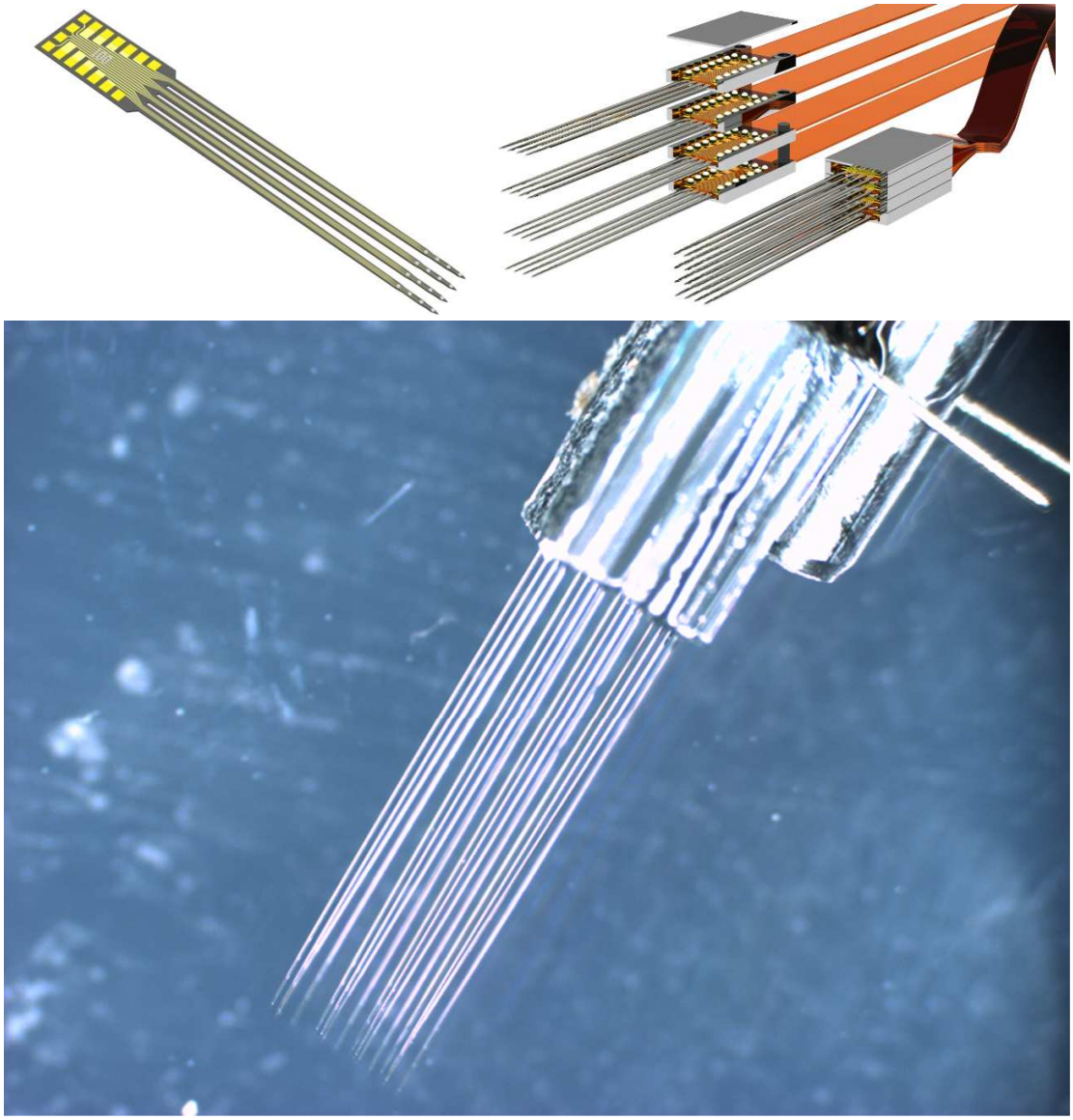

Figure V-1: Images of microfabricated silicon probes. (Top) Typical 2D Probe Design. These devices are then stacked together to create a three dimensional probe structure. (Bottom) Image of example 3D probe style as used in this study. The 4 rows of 4 shanks are spaced at 125 µm between shanks and each row of shanks is spaced at 300 µm.

B. *Surgery*

All implants in this study were performed on 250 - 300g female guinea pigs targeting primary auditory cortex. Surgical procedures were similar to those used previously (Vetter, Williams et al. 2004; Langhals and Kipke 2009; Ludwig, Miriani et al. 2009; Kim, Wiler et al. 2010). Initial anesthesia was administered via intraperitoneal injection of a mixture of 40 mg/kg ketamine and 5 mg/kg xylazine. Updates were given throughout the procedure every hour or as needed to maintain a consistent depth of anesthesia. To prepare the implant location, the surface of the head was first shaved and the skin and connective tissue on the surface of the skull were cleared. Next, three stainless steel bonescrews were secured in the skull anterior to bregma, and a bolt was then affixed to these screws using dental acrylic for the purpose of securing the head to a manipulator.

After securing the animal, a craniotomy approximately 4 x 4 mm was made over primary auditory cortex. The dura was resected in order to allow for probe insertion and the exact target was located using the well-defined vascular landmarks that have been reported previously(Hellweg, Koch et al. 1977; Langhals and Kipke 2009; Kim, Wiler et al. 2010). The 3D electrode array was then mounted to the stereotaxic manipulator and driven perpendicular to the cortical surface to a target depth of about 1 mm, so that the deepest electrode sites were located near layer IV. Last, a stainless steel needle was inserted into the skin tissue of the upper back and used as a reference and ground for all

recordings in the experiment. All procedures complied with the U.S. Department of Agriculture guidelines for the care and use of laboratory animals and were approved by the University of Michigan Animal Care and Use Committee.

C. *Electrophysiology*

All recordings were acquired using a TDT multi-channel acquisition system (RX5, Tucker-Davis Technologies, Alachua, FL) in an electrically and acoustically shielded booth. Neural electrophysiological recordings for all 64 channels were fed through an anti-aliasing filter (0.35 Hz – 7.5 kHz) amplified, and sampled at ~25 kHz. Wideband data for post-processing unit characterization was left unfiltered.

During all recording sessions, white-noise bursts, clicks, or individual tones generated by the TDT hardware were played through a closed-field speaker connected to the animal's ear in the sound-isolation booth. The amplitudes of all tones and clicks were adjusted based on a known calibration curve using the TDT PA5. White noise bursts were created by taking flat spectrum random noise and low-pass filtering the signal. These bursts were presented for 200 ms at two times per second to the subject. Clicks were generated of various amplitudes from 0 - 90 dB SPL and were presented to the subject 2-4 times per second. Each single frequency tone was presented for 100-200 ms at one to four presentations per second. Each tone was cosine gated on and off to avoid transient speaker clicks from step amplitude changes (Arenberg, Furukawa et

al. 2000; Kim, Wiler et al. 2010). Tone amplitudes ranged from 0 - 90 dB SPL and frequencies ranged from 500 Hz - 25 kHz. Tones were repeated multiple times to allow for signal averaging in the histograms. Spontaneous trials were randomly interspersed throughout the recording session where the attenuator was set to maximum resulting in 0 dB clicks or tones.

D. *Data Filtering and Analysis*

Wideband neural recording segments were analyzed off-line using custom automated MATLAB (Mathworks, Natick, MA) software, as described in detail elsewhere (Ludwig, Miriani et al. 2009; Rohatgi, Langhals et al. 2009). Briefly, an amplitude discrimination threshold was set at 3.5 standard deviations above and below the mean of the recording segments. For each peak exceeding the threshold, a 2.4-ms candidate waveform snippet centered on the absolute minimum of the waveform was removed from the recorded segment and stored. The peak-to-peak noise level was calculated as six times the standard deviation of the remaining data. After initial principal component analysis, individual clusters were identified using fuzzy c-means clustering. After clustering, waveforms with a cluster membership index of greater than 0.8 were used to determine a mean waveform for a cluster. The signal-to-noise ratio for these waveforms was calculated as the peak-to-peak amplitude of the mean waveform divided by the calculated noise value. Values of greater than 1.1 were considered quality units that were easily discriminable from the underlying noise floor.

E. *Frequency Response Analysis*

Peri-stimulus time histograms (PSTHs) are plots used to examine the occurrence of spikes surrounding a given event. In this study, PSTHs were created surrounding either click or tone onset. To generate a PSTH, the number of spikes occurring during 5 millisecond bins of time surrounding each tone onset was tabulated. For example, with tone onset at t=0, bins include 0-5 ms, 5-10 ms, 10-15 ms, etc. Given multiple presentations of each click or tone, neurons that are tuned to the click or tone frequency or amplitude will show an increase in firing following the onset of the stimulus.

Frequency response maps were generated by creating histograms of the action potential times surrounding each tone frequency and amplitude presentation. The total number of spikes in the first 20 bins following onset were averaged (100 ms of data). The spontaneous trials were used to calculate baseline data and the same 100 ms following a 0 dB onset were used to calculate the spontaneous rate of firing for that neural channel. The mean value of the response window was then normalized to the cumulative mean and standard deviation of the channel in the baseline period to calculate a z-score indicating significance of response. Finally, the response map was smoothed using a 5-point normalized 2D Gaussian convolution on all images.

III. Results and Discussion

High quality neural spike waveforms (see methods D) were recorded in all

sessions using the wide-band recording data. Quality neural action potentials were recorded on 43 of 64 sites immediately following device insertion, suggesting that if increased damage had occurred during insertion due to the larger footprint of the 3-D array, it was not substantial enough to prevent recordings. Mean waveforms output from the clustering algorithm are shown in Figure V-2. Signal-to-noise ratios shown ranged from ~1 for multi-unit activity up to 3.5 for well-isolated single units, indicating that signal quality was also comparable with typical unit activity recorded from 2D arrays(Ludwig, Miriani et al. 2009). Channels 40, 55, & 60 are representative of noise artifacts that were of sufficient amplitude to be sorted by the algorithm. These can be distinguished from normal action potentials through the shape of the waveform and were excluded from any calculations of channel activity or responses.

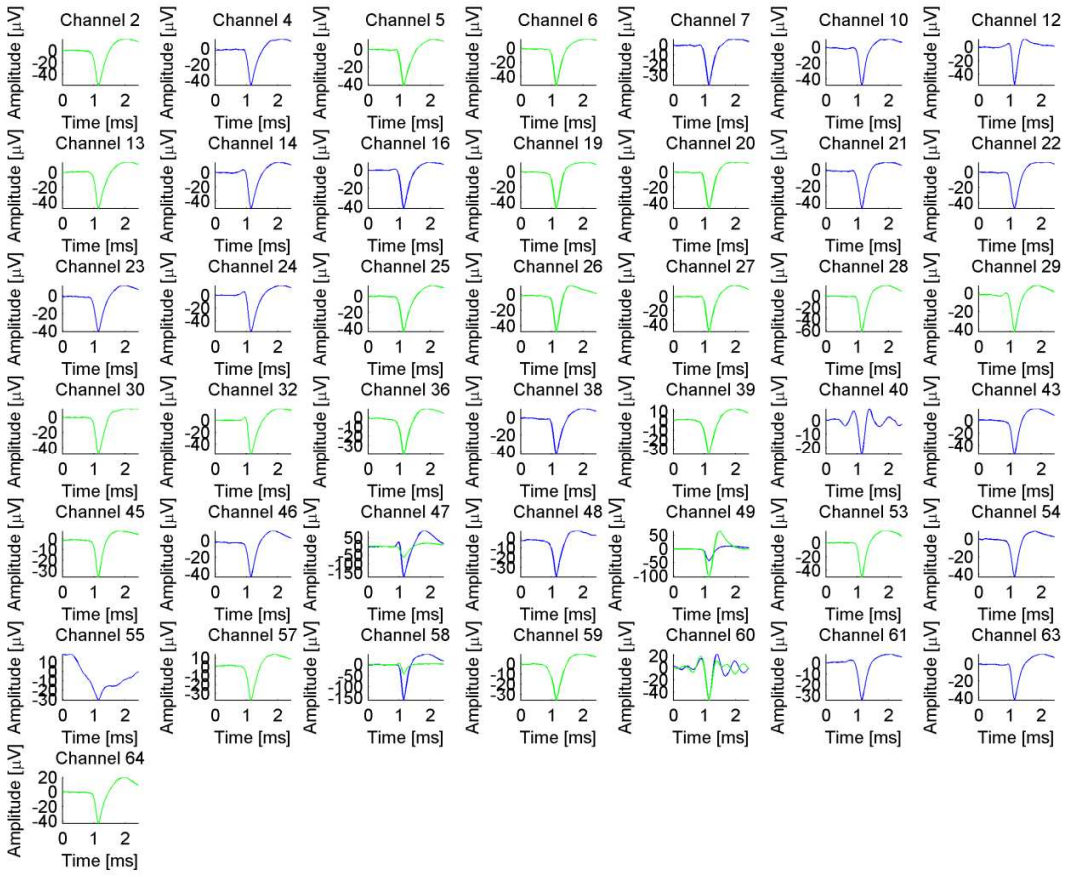

Figure V-2: Example mean spike waveforms of units recorded from the 3D array in GP3D-03 (Block-018). Different colored waveforms show that a number of channels have multiple unit waveforms present. The numbers above the plots indicate the signal-to-noise ratio of the presented mean waveform.

Individual channel activity was analyzed to examine the auditory-driven response characteristics of the implanted electrode arrays. White noise bursts trigger a delayed onset increase in neural firing rates recorded by electrodes implanted in the primary auditory cortex. Peri-stimulus time histograms of spike counts around the onset of the presented white noise burst are shown in Figure

V-3. All functional channels showed significantly large driven activity with an onset response that occurred 8-12 ms following the start of the presentation of the white noise, which is the expected delay arising from the number of synapses to the primary auditory cortex (Sally and Kelly 1988; Arenberg, Furukawa et al. 2000; Langhals and Kipke 2009; Kim, Wiler et al. 2010).

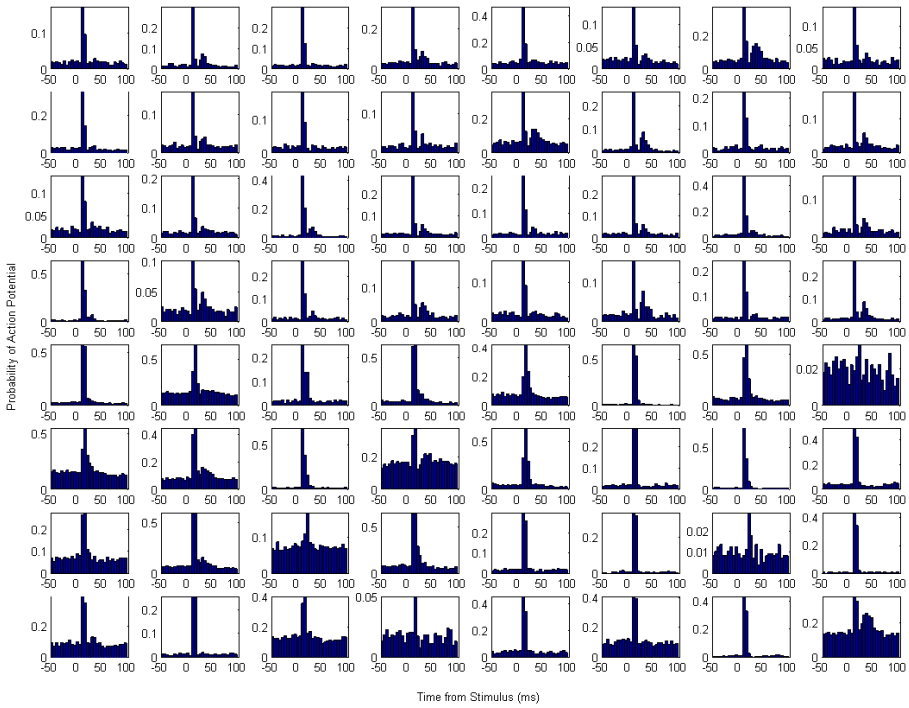

Figure V-3: PSTH's in response to 90 dB SPL Clicks. All 64 channels of activity, including MUA are shown. Tone onset is at t=0. Data for each channel ranges from 50 ms prior to tone onset up to 100 ms after. Some channels display a second firing peak approximately 20 ms following the initial onset response. At this high click intensity, the neuron fires a second action potential as soon as possible following the first response; the delay is due to the refractory period of the neuron.

In order to verify graded neural responses as is expected of primary auditory

cortical neurons, click thresholds were examined. In a given session, clicks of varying random amplitudes from 0 to 90 dB were presented to the subject and repeated up to 100 times(Kim, Wiler et al. 2010). A PSTH of each amplitude was then created for the total number of responses on each individual channel. The 50 ms period following tone onset was then summed for each channel to display the overall threshold response for the channel (Figure V-4). As can be seen in the upper panel of the figure, the example neural channel has an increased probability of firing at 45 dB, and the channel's peak response is nearly 1 at 90 dB, indicating that it fires a spike in that bin every time the click is presented. This is the typical result expected from a neuron / channel that is in auditory cortex; as higher intensity clicks are presented to a subject, the neuron’s firing rate increases until a plateau value is reach where it can no longer fire any faster.

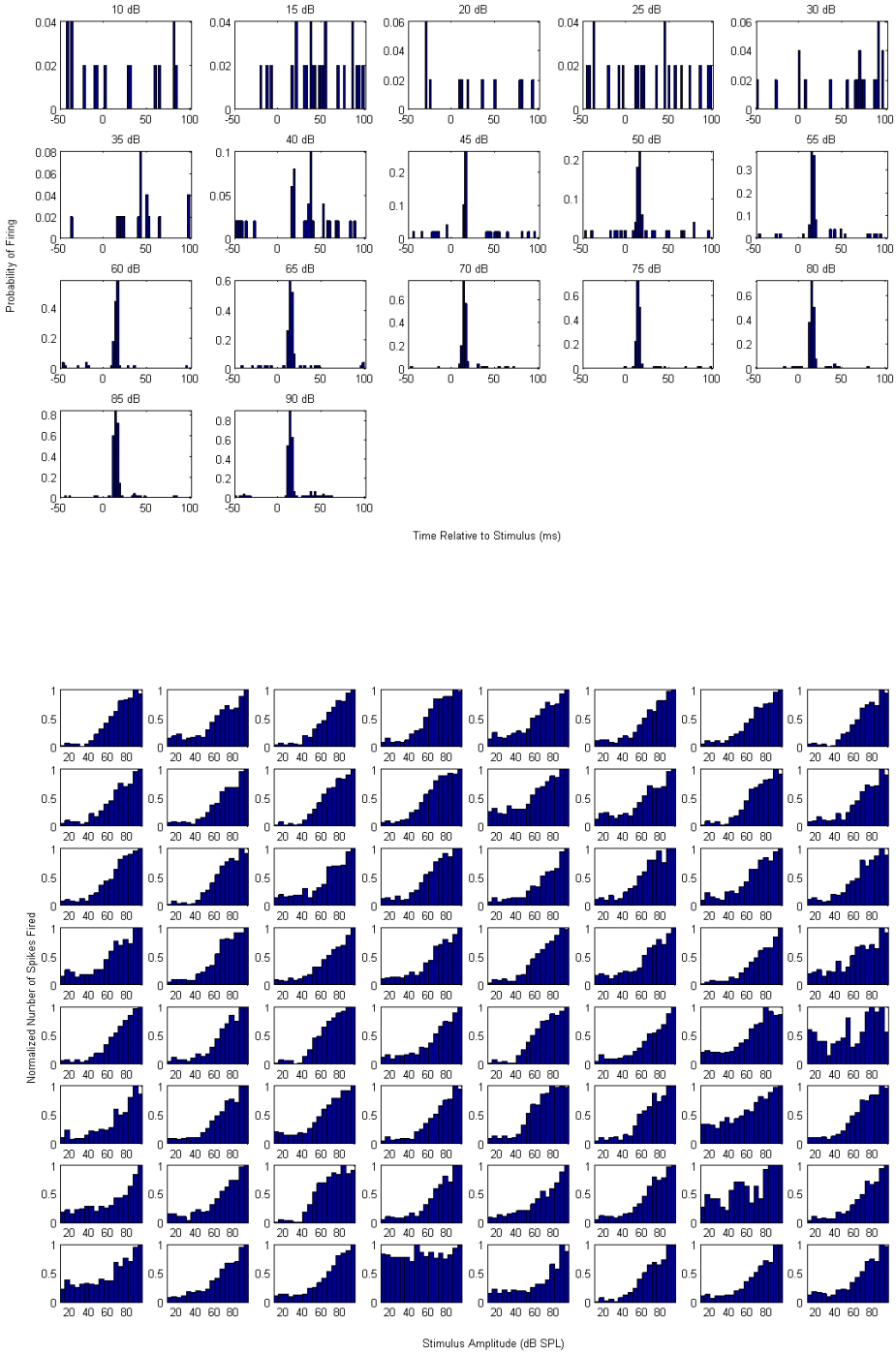

Figure V-4: (top) PSTH of a given responsive channel to clicks of increasing amplitudes from 10 - 90 dB. (bottom) aggregated responses of all 64 channels of the array to all click amplitudes in a given session.

We created frequency response maps to measure the tonotopic organization of the recorded units to evaluate the consistency of the tonotopic structure following device insertion. Figure V-5 shows example response maps covering two planes of electrode sites of the implanted 3D array. The best frequency for each of these maps was defined as the frequency that elicited a significant response of $p<0.01$ at the lowest threshold amplitude. The best frequencies for these electrodes ranged from about 0.9 kHz to 6 kHz.

All tonotopic maps suggest that 3D device insertion does not create substantially more damage from insertion than maps typically observed with the insertion of 2D arrays into the auditory cortex. Each functional electrode site recorded frequency-driven activity. Using the 3D electrode array in this study, we were able to successfully map a much larger region of the cortex than would have otherwise been possible through the use of a singular electrode or planar arrays.

Sites on an individual electrode 4x4 plane were similarly tuned to a specific frequency due to small site and shank spacing. However, electrodes on separate planes were tuned to different frequencies. Consequently, the use of a three dimensional probe with separate planes enables visualizing the tonotopic map of auditory cortex with 1 insertion, whereas the use of a 2-d probe would have required reinsertion and additional damage to orient the probe across the tonotopic gradient. In a chronic setting, this additional implant

damage could significantly impact long-term performance. Moreover, as electrodes have been demonstrated to move slightly with respect to the brain during chronic healing, a 3-d probe implant would have a higher likelihood of maintaining at least some of the electrodes on the array in the desired cortical location.

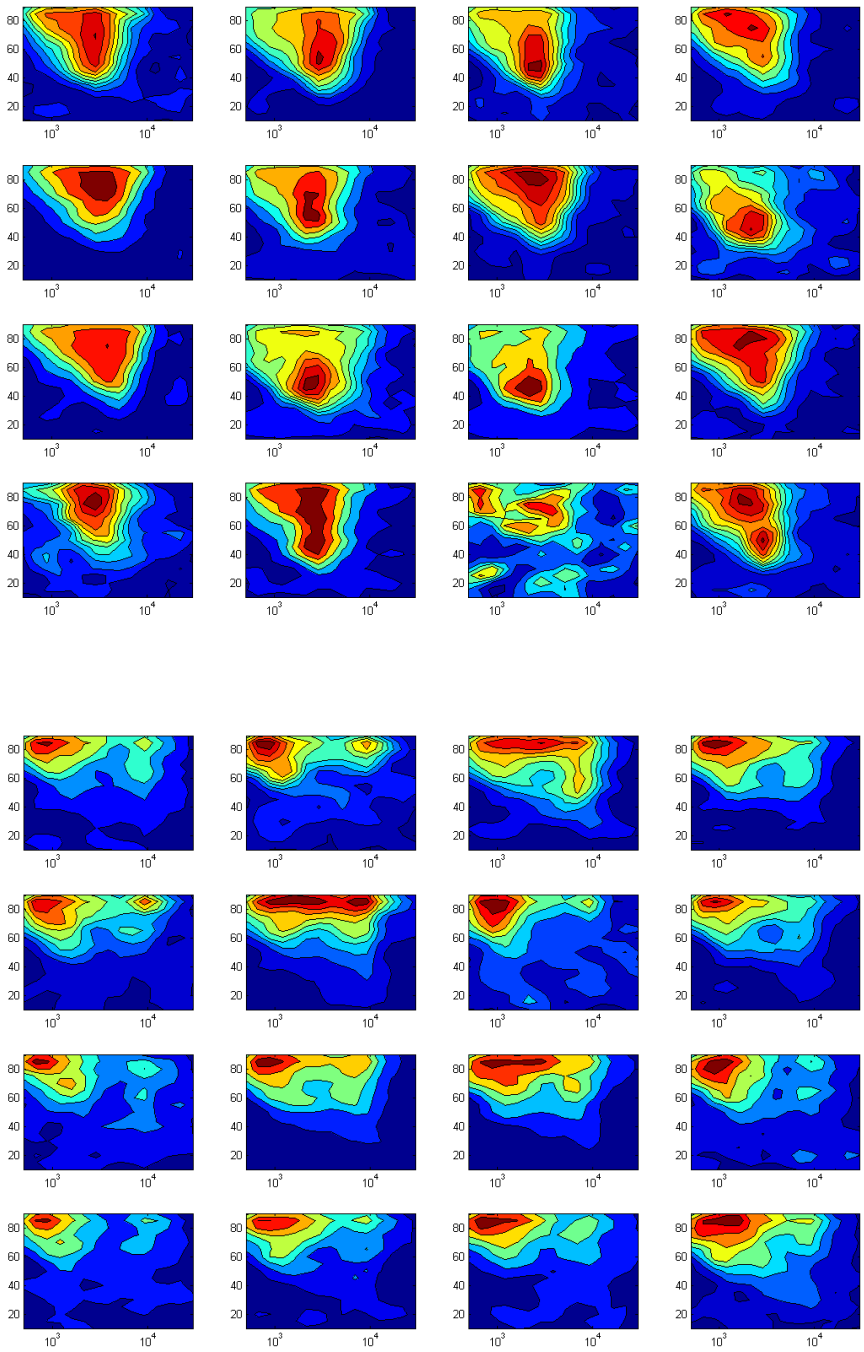

Figure V-5: Frequency response maps of the 2 end planes of 16 sites on the array. The x-axis is the frequency of the presented tone, the y-axis is the amplitude in dB SPL and color axis is indicative of the z-score for the individual frequency / amplitude combination. All data has been smoothed with a normalized 5x5 Gaussian window. All sites are organized by their spatial location. The best frequency of channels in the upper plane was between 3-6 kHz, while the lower plane of channels were tuned between 900 - 1200 Hz.

IV. Conclusions

In this study, we have provided proof of concept validation of a novel 3D architecture neural probe. The array was successfully inserted into the guinea pig cortex with neural recordings obtained soon following insertion, which suggests that the insertion trauma is comparable to conventional single or multi-shank microelectrode arrays. We recorded auditory-driven activity indicating that the neural circuits in the cortex remained intact. Finally, we measured frequency response maps showing that the tonotopic organization of auditory cortex is of the expected architecture. While we were able to record and characterize a large region of brain simultaneously, many of the maps showed little variability. Individual frequency response maps did not differ significantly between depths and in planes oriented perpendicular to the tonotopic map. However, the use of a multiple plane neural probe allows the brain to be mapped with a singular insertion, where a 2D probe would have required multiple insertions to orient the probe within the tonotopic space. These results combine to provide a solid, proof of concept validation of this 3D probe architecture. This work also promotes future studies directed at utilizing this technology to its fullest potential for exploring interconnectivity of neurons within the brain and mapping the neurophysiology of neural systems.

As one of the first 3D mapping probes utilized to date, this probe design can influence many features of next generation devices. Neuroprosthesis designs

are heavily dependent on the exact application for the device. Based on the results of this study, closely spaced electrode sites show primarily redundant information about the frequency response maps of the cortex. However, having two electrodes per shank may provide redundancy against device failure and elucidate features of non-perpendicular insertions. Overall, frequency response mapping of primary auditory cortex could be optimized through the use of electrodes spaced at least 300 microns with two electrodes per shank. This new device design could more efficiently acquire information about frequency borders through less electrode sites while still preventing device failure from yield issues. However, this is only one potential application of a 3D mapping array. While employing techniques such as spike-triggered averaging, electrodes spaced at 300 microns are less likely to provide the redundant information about neural morphology necessary for analysis. For that application, a more ideal probe design would include two facing planes of multiple shanks of electrode sites spaced as closely as possible. For any foreseeable application, three dimensional arrays have the potential to provide substantially more information about the underlying neurophysiology than possible with individual microelectrodes or their planar counterparts. Given that many applications have unique and specialized requirements, the best solution is a highly customizable and modifiable neuroprosthesis that can be adaptable to the specific neural interface environment to be mapped.

V. Acknowledgment

Takashi D. Y. Kozai, and Paras Patel for helpful discussions and paper review, and the rest of the Neural Engineering Lab at the University of Michigan.

VI. GRANTS

This work was supported by the NIH P41 Center for Neural Communication Technology (EB002030) and the Whitaker Foundation.

VII. DISCLOSURES

Daryl R. Kipke has significant financial interest in NeuroNexus Technologies, a leading supplier of microelectrode technology. Nicholas B. Langhals was a consultant for NeuroNexus Technologies.

VIII. References

Aarts, A. A., H. P. Neves, et al. (2008). "A 3D slim-base probe array for in vivo recorded neuron activity." Conf Proc IEEE Eng Med Biol Soc **2008**: 5798-5801.

Arenberg, J. G., S. Furukawa, et al. (2000). "Auditory cortical images of tones and noise bands." J Assoc Res Otolaryngol **1**(2): 183-194.

Blanche, T. J., M. A. Spacek, et al. (2005). "Polytrodes: high-density silicon electrode arrays for large-scale multiunit recording." J Neurophysiol **93**(5): 2987-3000.

Csicsvari, J., D. A. Henze, et al. (2003). "Massively parallel recording of unit and local field potentials with silicon-based electrodes." J Neurophysiol **90**(2): 1314-1323.

Du, J., I. H. Riedel-Kruse, et al. (2009). "High-resolution three-dimensional

extracellular recording of neuronal activity with microfabricated electrode arrays." J Neurophysiol **101**(3): 1671-1678.

Hellweg, F. C., R. Koch, et al. (1977). "Representation of the cochlea in the neocortex of guinea pigs." Exp Brain Res **29**(3-4): 467-474.

Kim, D. H., J. A. Wiler, et al. (2010). "Conducting polymers on hydrogel-coated neural electrode provide sensitive neural recordings in auditory cortex." Acta Biomater **6**(1): 57-62.

Kotter, R. and E. Wanke (2005). "Mapping brains without coordinates." Philos Trans R Soc Lond B Biol Sci **360**(1456): 751-766.

Langhals, N. B. and D. R. Kipke (2009). "Validation of a novel three-dimensional electrode array within auditory cortex." Conf Proc IEEE Eng Med Biol Soc **2009**: 2066-2069.

Lebedev, M. A. and M. A. Nicolelis (2006). "Brain-machine interfaces: past, present and future." Trends Neurosci **29**(9): 536-546.

Ludwig, K. A., R. M. Miriani, et al. (2009). "Using a common average reference to improve cortical neuron recordings from microelectrode arrays." J Neurophysiol **101**(3): 1679-1689.

Rohatgi, P., N. B. Langhals, et al. (2009). "In vivo performance of a microelectrode neural probe with integrated drug delivery." Neurosurg Focus **27**(1): E8.

Sally, S. L. and J. B. Kelly (1988). "Organization of auditory cortex in the albino rat: sound frequency." J Neurophysiol **59**(5): 1627-1638.

Schwartz, A. B. (2004). "Cortical neural prosthetics." Annu Rev Neurosci **27**: 487-507.

Ulbert, I., E. Halgren, et al. (2001). "Multiple microelectrode-recording system for human intracortical applications." J Neurosci Methods **106**(1): 69-79.

Vetter, R. J., J. C. Williams, et al. (2004). "Chronic neural recording using silicon-substrate microelectrode arrays implanted in cerebral cortex." IEEE Trans Biomed Eng **51**(6): 896-904.

Chapter VI

Conclusions and Future Directions

I. Conclusions

The work presented in this dissertation was focused on strategies for optimizing information extraction from cortical recordings. Optimizing the information extracted from neural recording electrodes is a key step in increasing the utility, reliability, and longevity of brain machine interfaces. The 4 studies comprising this dissertation demonstrate a framework that has been developed and utilized for developing and characterizing the next generation of neural interfaces. Through the use of objective classification algorithms, advanced information processing techniques, electrode site modifications, and multidimensional neural probes, we have taken the first step towards defining the requirements and metrics necessary to compare new interface technologies, and in turn develop a stronger understanding of the underlying structure and function of the brain.

Chapter 2 describes an automated, objective neural sorting and characterization toolbox that has been developed for the purposes of analyzing

neural data. While some commercial packages are capable of analyzing neural data similar to that presented in this chapter, our toolbox provides all of these features at no cost. Additionally, our toolbox includes additional features and is more accurate in spike classification due to objectively identified sorting parameter choices. We demonstrate specific instances where Offline Sorter classifies obvious noise as a neural spike cluster, whereas our algorithm correctly leaves the noise cluster unclassified. Our package is also capable of analyzing advanced waveform characteristics, signal levels, SNRs, and waveform changes over time, whereas commercial packages do not include these features. We have demonstrated, using simulated data, that our package correctly identifies spikes in both low and high noise environments. Since our package is an open-source solution, collaborative researchers can adapt it to their neural recording hardware or experimental apparatus for further customization. Our collaborators have already begun using this package in their experiments and have reported back with feedback that is influencing future designs.

In Chapter 3, we report on a novel data processing application for extracting information about neural morphology through the use of simultaneous recordings from spatially distinct electrodes. Within this study, we have recorded voltage perturbations from neurons at distances greater than 100 microns away from the site; this distance has been previously reported as the maximum distance a neuron can be recorded. By using this spike-triggered averaging technique, we have verified that neurons within the brain do not

behave as point sources, but instead have distributed voltage profiles arising from axonal and dendritic currents away from the cell body. Small voltage perturbations generated by axons/dendrites on electrodes distant from the soma are typically obscured by noise, but by using our technique we are able to average out the noise to reveal these signals. Through the use of known electrode locations in three dimensions, we have been able to image neural shapes and morphologies on a scale orders of magnitude smaller than functional magnetic resonance imaging, without the need for tissue slice or post implant histological techniques.

While the first two chapters are focused on neural signal processing for clustering and extracting useful features from the brain, Chapter 4 is instead focused on device modifications. We investigated using poly(3,4-ethylenedioxythiophene) (PEDOT) to lower the impedance of small, gold recording electrodes with initial impedances outside of the effective recording range. Smaller electrode sites enable more densely packed arrays, increasing the number of input and output channels to and from the brain. Moreover, smaller electrode sizes promote smaller probe designs; decreasing the dimensions of the implanted probe has been demonstrated to decrease the inherent immune response, a known contributor to the failure of long-term implants. As expected, chronically implanted control electrodes were unable to record well-isolated unit activity, primarily as a result of a dramatically increased noise floor. Conversely, electrodes coated with PEDOT consistently recorded high-quality neural activity, and exhibited a much lower noise floor than

controls. These results demonstrate that PEDOT coatings enable electrode designs 15 microns in diameter.

In Chapter 5, we validated a novel three-dimensional neural probe design by mapping guinea pig auditory cortex simultaneously in three dimensions. In this study, we also report auditory mapping experiments that include frequency response characteristics as a function of both cortical depth, as well as cortical location. While previous experiments required long sessions with multiple probe penetrations and separate recording files, this new probe design allows cortical mapping to be completed in a fraction of the time. Furthermore, the use of 3D probes such as the ones utilized here opens the doorway to future experiments examining neural connectivity and neurophysiological analysis which would otherwise have been extremely time consuming, if not impossible without high channel count, parallel-processed neural data.

II. Future Directions

While the four studies reported in this dissertation create a substantial step forward toward next generation neural interface systems, there are still many experiments that need to be completed before this technology is widely adopted. For an open-source automated spike classification algorithm to have the impact necessary to advance collaborative neural probe projects, more thorough beta testing must be completed. Currently, the software package has only been successfully tested using Tucker Davis Technologies and Plexon hardware-acquired data, but plans are currently underway to incorporate data

files recorded with Blackrock and Neuralynx systems. Once these have been completed, the software will be posted and distributed to provide a high-throughput neural data analysis solution through an open-source distribution platform.

Within the spike triggered averaging study, we demonstrated that information about neural morphology can be easily obtained using known firing times of action potentials from cortical neurons. Next generation analysis is currently underway to examine connections between neurons within the brain. Spike triggered averaging may also unearth neuronal connections that are typically obscured by noise. However, the variability in the exact timing between associated firing of first order connections will require large data sets and high voltage resolution recording systems.

In Chapter 4, we demonstrate that PEDOT can be used to create functional electrodes with diameters of less than 20 microns. We have recently utilized this technique to manufacture and test new devices within our research group. The initial development of our first generation neural probe design for decreased tissue encapsulation is below(Seymour and Kipke 2007). This first generation probe with small edge features lacked recording electrodes due to processing and impedance limitations. After completion of our study using small electrode sites functionalized with PEDOT, we utilized this technique on the development of even smaller gold electrode sites created on the face and edges of microfabricated polymer probes. This new electrode design publication

will be submitted in the near future and highlights a novel electrode design made possible by the work reported in this dissertation.

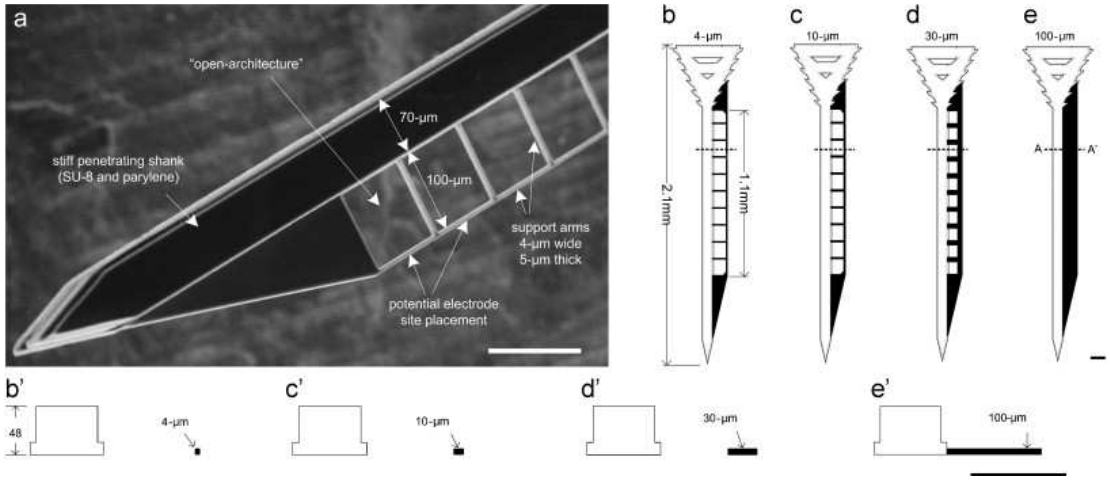

Figure VI-1: Figure 1 from (Seymour and Kipke 2007).

Also based on the foundation of our study employing PEDOT deposition onto small electrode sites to decrease impedance into a more acceptable range, we have recently developed a next generation microwire probe design using a carbon fiber backbone. These new electrodes were constructed from a 7 micron diameter carbon fiber, coated with parylene, and PEDOT was deposited on the tip to create the recording site. The first generation of these devices only used a carbon tip electrode site. While those probes were able to successfully record local field potentials, they were unable to differentiate single unit activity. It was only through the deposition of PEDOT that we were able to decrease site impedance of these devices to a level sufficient to minimize shunt loss and noise related to the impedance. This impedance decrease prevented neural signal attenuation that occurred with the carbon site devices so that high

quality, large SNR spikes could be recorded from the devices. A patent was submitted for this idea and it will be submitted to Nature Materials in the near future.

Future electrode designs will probably look nothing like current generation devices. Microwire arrays and silicon probes typically meet bare functionality requirements for most neural recording, electrophysiology, and brain machine interface applications. However, the yield on these devices tends to be too low to warrant wide-spread adoption of any one design. Further, human implantation of the "Utah" silicon array yielded insufficient success rates for brain machine interface applications. As mentioned above, ultra microelectrodes such as the carbon fiber probe may yield insight into the future designs, but these devices are still based on the fundamental concept of wire implanted from the surface of the brain. We are currently exploring the application of functionalized chemical coatings on the surfaces of the devices to increase biocompatibility. Ultimately for widespread adoption of the next generation neural probe, it will need to have a near 100% yield in useful signal, which will mean it will have to be an invisible stealth device that the brain doesn't even see. It is unclear how this can be achieved, but the more we understand how to create next generation probes and quantify their functionality, the more likely we will be able to develop some sort of tuned nanotechnology or manipulated biological machine that will solve all these neural recording issues.

III. References

Seymour, J. P. and D. R. Kipke (2007). "Neural probe design for reduced tissue encapsulation in CNS." Biomaterials **28**(25): 3594-3607.